Inhibition of oxidative stress in cholinergic projection neurons fully rescues aging-associated olfactory circuit degeneration in *Drosophila*

Ashiq Hussain[1]*, Atefeh Pooryasin[3]*, Mo Zhang[2]*, Laura F. Loschek[2], Marco La Fortezza[4], Anja B. Friedrich[1], Catherine-Marie Blais[1], Habibe K. Üçpunar[2], Vicente A. Yépez[5], Martin Lehmann[7], Nicolas Gompel[4], Julien Gagneur[5], Stephan J. Sigrist[3] and Ilona C. Grunwald Kadow[1,2,6]#

1 Technical University of Munich, TUM School of Life Sciences, Liesel-Beckmann-Str. 4, 85354 Freising, Germany

2 Max-Planck Institute of Neurobiology, Am Klopferspitz 18, 82151 Martinsried, Germany

3 Free University of Berlin, Institute of Biology, Neurogenetics, 14195 Berlin, Germany; Cluster of Excellence NeuroCure, Charité-Universitätsmedizin Berlin, 10117 Berlin, Germany

4 Ludwig-Maximilians-Universität München, Fakultät für Biologie, Biozentrum, Grosshaderner Strasse 2, 82152 Planegg-Martinsried, Germany

5 Technical University of Munich, Department of Informatics, Boltzmannstr. 3, 85748 Garching, Germany.

6 ZIEL – Institute for Food and Health, Technical University of Munich, 85354 Freising, Germany

7 Department of Molecular Pharmacology & Cell Biology, Leibniz-Forschungsinstitut für Molekulare Pharmakologie (FMP), 13125 Berlin, Germany.

Corresponding author: Ilona C. Grunwald Kadow, ilona.grunwald@tum.de

Abstract

Loss of the sense of smell is among the first signs of natural aging and neurodegenerative diseases such as Alzheimer's and Parkinson's. Cellular and molecular mechanisms promoting this smell loss are not understood. Here, we show that *Drosophila melanogaster* also loses olfaction before vision with age. Within the olfactory circuit, cholinergic projection neurons show a reduced odor response accompanied by a defect in axonal integrity and reduction in synaptic marker proteins. Using behavioral functional screening, we pinpoint that expression of the mitochondrial reactive oxygen scavenger SOD2 in cholinergic projection neurons is necessary and sufficient to prevent smell degeneration in aging flies. Together, our data show that oxidative stress induced axonal degeneration in a single class of neurons drives the functional decline of an entire neural network and the behavior it controls. Given the important role of the cholinergic system in neurodegeneration, the fly olfactory system could be a useful model for the identification of drug targets.

Main text

In order to exploit *Drosophila* to characterize the mechanisms of neural circuit degeneration, we first established that flies show a similar early aging-dependent decline in olfactory perception as humans (Doty et al., 1984). In olfactory T-maze assays, where the animal's preference or aversion for an odor is recorded as an index of their approach or avoidance behavior toward the odorant, we found that the performance to 8 different (3 attractive, 5 aversive) odors gradually declined with age (Figure 1A and Figure 1 – Figure Supplement 1A-D). This decline occurred also for behavior to odors that are detected independent of the canonical olfactory receptor ORCO (olfactory receptor co-receptor), and hence affected all tested odorants recognized by the three classes of olfactory receptors (ORs, ionotropic receptors (IRs), and gustatory receptors (GRs); Figure 1 – Figure Supplement 1E-I). By contrast, the fly's high attraction to

53 blue light was not significantly different between 1 and 10 weeks of age (Figure 1B) indicating
54 that the flies were healthy enough to move and to make decisions in this type of behavioral
55 assay. These data argue that in flies, as observed in humans, the sense of smell declines
56 before and/or faster than the sense of vision.
57
58 We next sought to identify the underpinning neuronal and genetic mechanisms. First, we asked
59 whether all neurons were affected equally or whether perhaps particular neuron types within the
60 olfactory circuit were primary targets of aging. The architecture of the fly olfactory system
61 parallels that of vertebrates (Wilson, 2013). Olfactory sensory neuron (OSN) axons connect to
62 the antennal lobe (AL), the equivalent of the olfactory bulb (OB), in the brain, where olfactory
63 information is further processed and transferred by second order projection neurons (PNs;
64 analogs of mitral and tufted cells) to higher brain centers (Figure 1C). A straightforward reason
65 for a loss of sense of smell could be a loss of OSNs or a reduction in their odor responsiveness,
66 for instance through diminished olfactory receptor expression. Yet, by counting the number of a
67 subclass of OSNs we found no difference in the number of sensory neurons between young and
68 older flies (e.g., 1 week vs. 10 weeks *Or42b-Gal4; UAS-mCD8GFP* flies*;* Figure 2 – Figure
69 Supplement 1A), suggesting that OSNs do not die during aging. Furthermore, we detected no
70 significant difference in the size of OSN cell bodies between young and old flies (Figure 2 –
71 Figure Supplement 1B). In agreement with these data, RNA-sequencing (RNA-seq) of whole
72 antennae demonstrated that olfactory receptor expression including the expression of those
73 responding to the tested odors and the obligatory co-receptor ORCO, which is required for the
74 detection of the majority of odors, was not significantly different between young and old flies
75 (Figure 2 – Figure Supplement 1C,D).
76 We next investigated possible changes in the OSN's ability to respond to an odor, by recording
77 spikes of neuronal activity in single sensillum recordings, where an electrode is inserted into
78 individual olfactory sensilla (SSR; Figure 2 – Figure Supplement 2A). While the response to two

79 aversive odors, benzaldehyde and CO_2 showed a significant decrease in the number of elicited
80 spikes, none of the other recordings using other odorants (6 odors) showed a similar decline
81 (Figure 2 – Figure Supplement 2B-H). This result did not change even when flies were first
82 sorted by their response to the odor in the T-maze behavioral assay. Flies that reacted to the
83 odorant and flies that appeared to not care showed similar SSR responses, which were also not
84 significantly different between the age groups (Figure 2 – Figure Supplement 2J,K). Given that
85 the behavior to odors without a decline in SSR was similarly affected as the behavior to
86 benzaldehyde and CO_2, we concluded that a decrease in OSN sensitivity is unlikely to be the
87 general reason for the observed ageing-associated decline in olfactory behavior. Altogether
88 these experiments suggested that a degeneration of peripheral sensory neurons is not the
89 primary reason for the observed ageing-associated phenotype.
90
91 OSNs transmit their information to PNs in the central brain (~30 OSNs to one PN; Figure 1C).
92 The majority of PNs are cholinergic and can be labeled with the transgenic reporter line GH146-
93 Gal4 (Figure 2A). To test whether PNs were functionally impaired, we used *in vivo* calcium
94 imaging (*GH146-Gal4; UAS-GCaMP3.0*) as a proxy of neuronal activity. We first recorded
95 fluorescence changes at the level of the AL, where the dendrites of these neurons receive input
96 from the OSNs, using epifluorescence microscopy (Figure 2B). The PN odor response in the
97 responsive glomeruli was significantly reduced at different concentrations including those used
98 in the behavioral assays (1 mM, Figure 2B). With the exception of very few odors such as CO_2,
99 most odors activate multiple glomeruli. To better distinguish glomerulus-specific responses, we
100 turned to two-photon microscopy and imaged GCaMP fluorescence changes at three different
101 levels of the AL (Figure 2C,D). Here, we observed that not all glomeruli were equally affected.
102 While for each odor, one, normally very responsive glomerulus showed a strong and significant
103 decline, two other glomeruli were not significantly affected by age (Figure 2C,C',D,D'). The
104 reason for why different glomeruli are differentially affected is not know at this point. Differences

105 in OSN number or olfactory receptor expression can, according to the data shown above, likely
106 be excluded. Currently, we can only speculate that the degree of innervation by inhibitory or
107 excitatory local neurons in the AL, other distinctive features or the activity of the OSN-PN
108 synapses, interaction between sister PNs, or even the interaction with glia cells might play a role
109 in these differences. Nonetheless, the current data strongly suggest that, in contrast to OSNs,
110 PNs are less activated by odors in old as compared to young flies.
111
112 PNs transfer their information mainly to two higher brain centers, the MB calyx and the LH. To
113 characterize PN function further, we also imaged GCaMP fluorescence changes at the level of
114 PN boutons in the calyx (Figure 2E-G). Remarkably, here the response per PN bouton was not
115 significantly weaker between flies of different ages (Figure 2F). However, the number of
116 responsive boutons was strongly reduced in old (4, 6 weeks) as compared to young flies (1
117 week; Figure 2G. Therefore, PN function is affected by aging. Importantly, not only their
118 dendritic response is reduced in a glomerulus-specific manner, their axonal output to higher
119 brain centers drastically diminishes with age. The strength of this decline indicates that primarily
120 axons and their synaptic output regions might degenerate functionally or anatomically due to
121 aging-related mechanisms.
122
123 These cellular data suggested that flies suffer from reduced odor sensitivity possibly due to a
124 decline of PN function and a subsequent reduction in information that arrives at higher brain
125 centers. Hence, we wondered whether the animals were still be capable of odor recognition and
126 valuation, if compensated for the loss in sensitivity. Indeed, a 10-fold increase in odor
127 concentration was sufficient to markedly improve the old flies' olfactory choice behavior
128 indicating that old flies albeit a decline in odor sensitivity still recognize and correctly valuate a
129 given odor (Figure 2 – Figure Supplement 3).
130

131 To unravel the mechanism of this functional decline, we analyzed PN morphology in more detail
132 (Figure 3A). In contrast to OSNs, the number of PNs labeled by the reporter GH146>mCD8GFP
133 was mildly but significantly reduced in old as compared to younger flies (Figure 3B). In addition
134 to the mild loss of labeled PNs, their cell bodies had shrunk in older animals as compared to
135 younger animals (Figure 3C). Similar observations were made for other aging neurons including
136 mitral cells in aged humans (Sama ul et al., 2008). Importantly, the pan-neuronally expressed
137 gene *elav* was somewhat upregulated relative to other genes in older brains as compared to its
138 relative expression in younger brains (Figure 3F) suggesting that neurons were not selectively
139 lost in larger numbers as compared to other cell types (e.g. glia) in aging *Drosophila* brains.
140 Nevertheless, we observed a significant decrease in ToPro staining, which labels cell nuclei in
141 several areas including the AL (Figure 3G,H). Despite of this, the expression level of the
142 neuropil marker N-cadherin (Ncad) in the AL and in the region of the LH as judged by antibody
143 staining was unchanged (see methods; Figure 3D). Similarly, the expression of the GCaMP
144 reporter (normalized to Ncad staining) used for calcium imaging, was comparable, or even
145 slightly increased in PN axon terminals of old as compared to young flies (Figure 3E).
146 Therefore, the changes observed in PN odor responses are not likely to be attributable to gross
147 morphological changes in PN anatomy.
148
149 We next focused on expression and localization of markers of neuronal function to pinpoint a
150 cellular defect in the PNs that could explain the observed functional decline. As a reduction in
151 cholinergic signaling accompanies most forms of neurodegeneration and natural aging (Doty,
152 2012), and because PNs are cholinergic, we analyzed the expression of genes involved in
153 cholinergic neurotransmission with RNA-sequencing. Our analysis revealed a significant decline
154 in mRNA abundance of several Acetylcholine receptor (AChR) subunits (Figure 3F). By
155 contrast, some previously implicated marker genes of systemic aging and lifespan did not
156 change or increased in their expression (Figure 3F). Expression levels are only one factor that

157 might impact on cellular function. The proper transport and localization of relevant proteins
158 represents another critical point. As a proxy for synaptic integrity of the PNs, we expressed
159 transgenic reporter constructs producing synapse-localized fluorescent marker proteins. Such a
160 reporter construct for the localization of Acetylcholine receptors expressed in PNs
161 (GH146>Dα7-GFP) revealed a moderate, but significant signal reduction of this postsynaptic
162 marker at PN postsynaptic sites in the AL indicating an aging-related change at the post-
163 synapse (Figure 3G,I).
164
165 It has been proposed that axonal degeneration precedes and possibly leads to eventual
166 neuronal loss in neurodegenerative diseases (Kurowska et al., 2016). Indeed, we observed that
167 the Dα7-GFP reporter construct, which in young animals localizes not only to the post-synapse,
168 but also, albeit to a markedly lower extend, to the axon and presynaptic terminals of PNs (in
169 20/20 animals analyzed) was completely absent from presynaptic terminals and axons in old
170 flies (0/20 flies showed reporter labeling in axon, MB calyx (cx) and lateral horn (LH)) (Figure
171 3G). In mammals, AChRs are also found post- and pre-synaptically, where they modulate and
172 enhance synaptic signaling (MacDermott et al., 1999).
173
174 Given the dramatic reduction of responsive presynaptic PN boutons in the MB calyx and the
175 reduced response in the AL observed by GCaMP imaging (see Figure 2), we employed
176 antibody staining against the enzyme ChAT (Choline Acetyltransferase) required for the
177 production of Acetylcholine at synapses of cholinergic neurons such as the PNs. Quantification
178 of these stained brains indeed revealed a significant reduction in ChAT positive puncta in the AL
179 and at the level of the MB calyx (Figure 3J-L). ChAT staining in the LH, by contrast, remained
180 relatively stable (Figure 3L). Beyond a change in synaptic proteins in the aged synapse, several
181 studies in animal models including flies implicated mitochondrial dysfunction in neuronal, in
182 particular axonal degeneration (Court and Coleman, 2012; Humphrey et al., 2012; Valadas et

183 al., 2015). The current hypotheses for why axonal mitochondria are more vulnerable include the
184 remote location of mitochondria in presynapses from the cell body, and a high metabolic activity
185 including calcium homeostasis (Court and Coleman, 2012). Indeed, we observed a strong
186 reduction in the number of puncta that were positive for a reporter construct for mitochondria
187 (GH146>mito-mcherry; (Vagnoni and Bullock, 2016) at the level of the MB calyx (Figure 3K,L),
188 but not in the AL or LH area (Figure 3J,L). These results suggests that mitochondria are indeed
189 depleted, lost, or not replenished selectively close to the remote synapse in the calyx, while
190 postsynaptic sites of the PNs in the AL are seemingly maintained. Why LH synapses are not
191 affected as compared to calyx synapses, given that they are actually further away from the cell
192 bodies than their calycal counterparts, remains currently unknown. Nevertheless, specific
193 metabolic or synaptic characteristics of these different synapses and their postsynaptic partners
194 could be part of the explanation.
195
196 In the light of an apparent reduction of ChAT and mitochondria (or at least a mitochondria
197 reporter), we analyzed the integrity of these boutons in more detail using the high-resolution
198 microscopy technique STED (Stimulated emission depletion; (Kittel et al., 2006; Willig et al.,
199 2006)). To this end, the expression of a GFP-tagged version of the presynaptic protein
200 bruchpilot was expressed in PNs (GH146>short-brp-GFP; Figure 3M). In line with the strong
201 reduction of odor-responsive boutons, quantitative STED analysis of this reporter revealed a
202 strong decrease in the density of presynaptic active zones over the MB calyx (Figure 3N).
203 Correspondingly, the number of postsynaptic densities as revealed by antibody staining against
204 the postsynaptic density marker Drep2 was reduced by a similar margin (Figure 3O) (Andlauer
205 et al., 2014).
206
207 These data indicate that a degeneration of cholinergic PNs, in particular of the axon, the
208 presynaptic boutons and the corresponding synapses (i.e. active zones and postsynaptic

209 densities), resembling aspects of neurodegeneration in humans, could be involved in the loss of
210 the sense of smell.
211
212 Having identified a potential neuronal target of aging in the olfactory system, we next addressed
213 the genetic mechanisms underpinning aging-associated olfactory decline. Several key genes
214 and mechanisms have been identified in different model systems that contribute to systemic
215 aging (Lopez-Otin et al., 2013). To assess the mechanism of olfactory aging in our case, we
216 used *in vivo* RNAi to knock-down the expression of candidate genes previously implicated in
217 systemic aging and lifespan in the entire nervous system using a pan-neural transgenic driver
218 line, *elav-Gal4*, or loss of function mutants. Of the ~20 genes analyzed the knock-down of only
219 one gene, only *SOD2* (mitochondrial form of superoxide dismutase) significantly affected
220 olfactory behavior in young animals (Figure 4A; Figure 4 – Figure Supplement 1A,B). By
221 contrast, knock-down of the cytoplasmic form, *SOD1*, only resulted in a smaller but non-
222 significant decrease in olfactory behavior (Figure 4A). Sirt2 RNAi knock-down led to a mild, but
223 not significant increase in odor attraction, possibly reflecting the fact that Sirt2 is upregulated in
224 older brains (Figure 4A). More generally, it will be interesting to test overexpression of genes
225 upregulated in aged brain for their role in neurodegeneration in the future.
226
227 SODs protect against reactive oxygen species (ROS) and SOD2 appears to be required for
228 normal lifespan (Kirby et al., 2002; Oka et al., 2015). Our RNA-seq data revealed that while
229 *SOD1* and *SOD2* expression remained unchanged in the antennae of old flies, both genes were
230 expressed at lower levels in older brains (Figure 4 – Figure Supplement 2A-C).
231 In addition to SOD1 and SOD2, other genes were significantly up- and downregulated in older
232 brains. Among the most significant up-regulated GO terms were proteolysis and
233 defense/immunity genes, while energy metabolism and oxidation process related genes ranked
234 high in the list of downregulated genes. For instance, genes belonging to the GO term

235 ‘oxidation-reduction process’ were found to be significantly downregulated (FDR <0.01), which
236 corresponds to 128% more genes than expected by chance (P=2.3e-14, Fisher Test). Similarly,
237 119 genes belonging to proteolysis GO term were found to be significantly upregulated
238 (FDR<0.01), which corresponds to 59% more genes than expected by chance (P=1.3e-8,
239 Fisher Test) (Supplementary File 1 and 2). These results were also well in line with our finding
240 of a reduction of mitochondria in PN synapses (see Figure 3).
241
242 We next tested whether any particular neuron type in the olfactory system was most vulnerable
243 to oxidative stress, or whether this was a systemic effect. Notably, knock-down of *SOD2* in
244 OSNs (ORCO-Gal4) had no effect on the flies’ olfactory attraction or aversion compared to
245 genetic controls (Figure 4B). By contrast, knock-down of *SOD2* in PNs resulted in a significantly
246 reduced odor attraction and odor aversion similar to the knock-down of *SOD2* in all mature
247 neurons (Figure 4C and Figure 4 – Figure Supplement 2D). While ubiquitous or pan-neural
248 knock-down of *SOD2* with the same construct as used here is lethal (flies die after ~3 days;
249 (Kirby et al., 2002) and our own observations), knock-down of *SOD2* in PNs did not reduce the
250 flies’ life span significantly as compared to the genetic controls, which were also used in the
251 behavioral experiments (Figure 4 – Figure Supplement 3A). It is important to note, however, that
252 given the well-known effects of genetic background on lifespan, we limit our conclusion to the
253 correlation of the lifespan of each individual test or control group to their respective olfactory
254 behavioral performance. In other words, an extremely short- or long-lived animal might show
255 unspecific reasons for behavioral deficits or improvements. Based on this, a reduced lifespan is
256 unlikely to explain the strong behavioral phenotype, suggesting a high vulnerability of PNs and
257 their central role in olfactory decline.
258
259 Does lack of SOD2 in PNs result in changes at the level of neuronal function and morphology
260 similar to what we observed for natural aging? To answer this, we carried out some of the same

261 analysis as done for aged flies (see Figure 2 and 3). First, we counted the number of PNs in 1
262 week old flies where SOD2 was knocked-down under the control of GH146-Gal4
263 (GH146>SOD2i). In contrast to the aged flies, the number of GCaMP reporter expressing PNs
264 (GH146>GCaMP; with or without SOD2i) was not significantly different between the
265 experimental group and controls (Figure 5A,B). However, the size of the PN cell bodies was
266 significantly smaller upon knock-down of SOD2 as compared to controls (Figure 5C), similar to
267 the decline of cell body size in old flies (see Figure 3). Quantification of the expression GCaMP
268 stained with an anti-GFP antibody in the LH and calyx revealed a small reduction, which was
269 significant in the LH but not in the calyx, suggesting that the relative expression level of GCaMP
270 upon normalization to staining outside the LH and calyx, respectively, remained at a similar level
271 as compared to controls (Figure 5D). By contrast, antibody staining against ChAT showed that
272 the expression of this enzyme was significantly reduced in PN boutons in the MB calyx (Figure
273 5E) indicating a reduction of functional cholinergic synapses – again in line with the results in
274 aged brains.
275 Next, we tested what the consequences of SOD2 lack meant for PN function by using two
276 photon *in vivo* calcium imaging of the PN boutons in the MB calyx (Figure 5F-H). While SOD2
277 knock-down did not affect the responses of individual PN boutons to odor stimulation, the
278 number of responsive boutons was significantly reduced upon SOD2 knock-down in PNs
279 (Figure 5G,H).
280 Taken together, reduction of SOD2 expression exclusively in PNs leads to behavioral, functional
281 and anatomical phenotypes that resemble several of the phenotypes observed in naturally aged
282 brains.
283
284 Systemic SOD2 overexpression can ameliorate memory deficits in a transgenic Alzheimer's
285 disease mouse model (Massaad et al., 2009). However, it is not known whether augmenting
286 SOD2 exclusively in one neuron type, the so to speak potential seed or Achilles heel of

287 degeneration, prevents aging-associated decline of an entire circuit and its ability to control and
288 drive behavior. We found that overexpression of SOD2 exclusively in PNs fully rescued
289 behavioral decline of 7 weeks old flies, which behaved just like their 1 week old genetic
290 counterparts (Figure 6A and Figure 6 – Figure Supplement 1A). Importantly, SOD2
291 overexpression in PNs did not significantly extend or shorten the average lifespan of this group
292 of flies as compared to the used genetic controls, which were also used for behavioral analysis
293 (Figure 4 – Figure Supplement 3B). Although these results do not allow strong conclusions
294 regarding the effect on lifespan, they do, nevertheless, indicate a more specific role of SOD2 in
295 PNs, and that the behavioral improvement is unlikely to be a result of an improved overall
296 fitness of these animals. Furthermore, SOD2 expression under the control of ORCO-Gal4 in
297 OSNs did not rescue the behavior of old flies (Figure 6B and Figure 6 – Figure Supplement 1B).
298 We conclude that cholinergic PNs represent key targets and possibly a 'seed neuron' population
299 in aging-associated decline of the sense of smell. These results suggest that aging-related
300 degeneration and behavioral decline could be significantly delayed by preventing oxidative
301 damage in only one or few neuron types (see also (Seeley, 2017)).
302
303 The overexpression of SOD2 does currently not provide a feasible way to protect the nervous
304 system of humans during aging or during the onset or course of a neurodegenerative disease. A
305 popular idea is that it might be possible to boost an organism's ability to fight ROS by
306 consuming a diet high in antioxidants (Vaiserman and Marotta, 2016). We found that a diet high
307 in Resveratrol, a well-studied antioxidant shown to increase the expression of SOD2 in neurons
308 (Fukui et al., 2010) and with potential benefits against AD (Granzotto and Zatta, 2014),
309 protected from olfactory decline. The relatively small effect on the flies' lifespan (Wood et al.,
310 2004) (Figure 4 – Figure Supplement 3C) is unlikely to explain the observed behavioral
311 improvement (Figure 6C and Figure 6 – Figure Supplement 1C). Notably, a 1 week Resveratrol
312 treatment of younger flies did not affect olfactory behavior as compared to solvent fed flies

313 (Figure 6 – Figure Supplement 1D) indicating that Resveratrol might indeed counteract oxidative
314 stress that builds up during aging. Thus, protection from oxidative stress, plausibly at least in
315 part through protection of PNs, might help to maintain the function of the olfactory system in an
316 aged individual.
317 Apart from certain diets and nutrients, the gut microbiome has been implicated in progression of
318 Parkinson's disease and aging (Kong et al., 2016; Scheperjans et al., 2015). Recent studies
319 show that beneficial effects of microbiota are conserved between *Drosophila* and mouse
320 (Schwarzer et al., 2016). For instance, the effects of malnutrition can be partially overcome by
321 inoculating flies with a specific strain of *Lactobacillus plantarum* (*L.p.WJL*) or *Acetobacter*
322 *pomorum* (*A.p.*) *(Schwarzer et al., 2016)*. Importantly, another strain of *L. plantarum*
323 (*L.p.NI202877*) did not produce the same effect suggesting a specific mechanism and not just
324 the presence of any bacteria in the gut. Oral administration of *L. plantarum*, which colonizes the
325 mammalian gut, led to a significant increase of SOD levels in serum and liver in a mouse aging
326 model (Tang et al., 2016). Moreover, *L.p.WJL* modulates TOR and insulin signaling in
327 *Drosophila*, both of which are regulators of lifespan (Storelli et al., 2011). We tested the effect of
328 these microbiota on olfactory aging. *L.p.WJL* and *A.p.*, but not *L.p.NI202877*, improved the old
329 flies' performance in olfactory preference assays significantly (Figure 6D and Figure 6 – Figure
330 Supplement 1E). We conclude that certain microbiota have a positive effect and slow-down
331 aging-associated olfactory neurodegeneration.
332
333 Based on the data presented, we propose that due to their insufficient resistance to oxidative
334 stress, which is facilitated by an aging-associated decrease in SOD levels, functional
335 degeneration starting at the axon of specific cholinergic neurons is responsible for the decline of
336 the olfactory circuit and the sense of smell (Figure 6E). A central role of cholinergic neurons in
337 neurodegeneration seems conserved. In *C. elegans*, a decline in cholinergic signaling likely
338 triggers an aging-associated decline in the sense of smell (Leinwand et al., 2015). In humans,

339 cholinesterase inhibitors, which augment levels of acetylcholine in the brain, represent the main
340 class of Alzheimer drugs (Canter et al., 2016). Using the *Drosophila* model, we showed that a
341 specific type of cholinergic neurons plays a key role in the loss of the sense of smell. Our data
342 therefore provides experimental evidence that declines in nervous system function are not due
343 to a universal degeneration, but rather that specific neuronal subsets are primarily or even
344 solely responsible and might trigger further degeneration throughout a neuronal network.
345 Why are certain neurons more sensitive than others? Similar to flies, axonal degeneration and
346 decline of cholinergic neurotransmission play important roles in neurodegeneration in humans.
347 Indeed, neurons with long axonal projections, broad input, high sensitivity and high action
348 potential frequency, such as PNs (Wilson, 2013), might be particularly vulnerable to aging. The
349 olfactory system of the fly could help to pinpoint the 'Achilles heel' of a neuron and aid the
350 development of more targeted treatments by combining high-throughput genetic screening with
351 drug or microbiota treatments.
352
353 **Acknowledgements** We would like to thank members of the Grunwald Kadow lab for critically
354 reading the manuscript. We thank Francois Leulier for bacterial strains and for consultation and
355 advice. We thank Jonathan Landry and the EMBL sequencing core facility for RNA-sequencing
356 and initial analysis, and Vicente Yepez for help in deeper transcriptome analysis. We would like
357 to acknowledge the contribution of Kaida Ning in the initial analysis of the RNA-sequencing data
358 of the fly antenna. This work was funded by the Max-Planck-Society, an EMBO young
359 investigator grant and an ERC starting grant to I.G.K., and by the Juniorverbund in der
360 Systemmedizin 'mitOmics' (FKZ 01ZX1405A J.G and V.A.Y).
361
362
363 **Competing financial interests** The authors declare no competing financial interests.

364 **Materials and Methods**

365 **Key resources: Fly Rearing and Lines**

366 *Drosophila melanogaster* stocks were raised on conventional cornmeal-agar medium at 25℃
367 temperature and 60% humidity and a 12 h light:12 h dark cycle. The following fly lines were
368 used to obtain experimental groups of flies for the different experiments:

369 1. *Canton S*
370 2. *w^{1118}*
371 3. *Or42b-Gal4 (Bloomington stock (BL) # 9971)*
372 4. *UAS-mCD8GFP (gift from L. Zipursky)*
373 5. *GH146-Gal4 (gift from L. Zipursky)*
374 6. *elav-Gal4;UAS-Dcr-2 (BL# 25750)*
375 7. *RNAi: UAS-SOD2i (Bloomington stock (BL) # 24489; (Kirby et al., 2002)), UAS-SOD1i*
376 *(BL# 24493), UAS-TORi (BL# 33627), UAS-InRi (VDRC ID 992), UAS-Sirt2i(a,*
377 *BL#31613), UAS-Sirt2i(b, BL# 36868), UAS-Indyi (VDRC ID 9981) , UAS-chicoi (BL#*
378 *28329), UAS-mthi (BL# 27495), UAS-FOXOi (VDRC ID 107786), UAS-FMR1i (BL#*
379 *27484)*
380 8. *UAS-SOD2 (BL# 24494)*
381 9. *nsyb-Gal4 (gift from L. Zipursky)*
382 10. *UAS-GCaMP3 (gift from S. Sachse)*
383 11. *ORCO-Gal4 (BL# 23292)*
384 12. *$Orco^{1}$ (BL# 23129)*
385 13. *UAS-Dα7-GFP (gift from G. Tavosanis)*
386 14. *UAS-BRP-$short^{GFP}$ (Christiansen et al., 2011; Kremer et al., 2010)*
387 15. *y[1], Atg8a[d4] (from (Pircs et al., 2012))*
388 16. *w[1118]; Atg7[d77] (from (Juhasz et al., 2007))*

389

390 The lines were obtained from Bloomington (http://flystocks.bio.indiana.edu/) or the Vienna
391 Drosophila Resource Center (VDRC) stock center (http://stockcenter. vdrc.at) unless indicated
392 otherwise.
393
394 **Further key resources**
395 1. Resveratrol (Sigma-Aldrich, R5010)
396 2. *Lactobacillus plantarum* or *Acetobacter pomorum* (all strains were a gift of Francois
397 Leulier)
398 3. Antibodies and additional reagents used for molecular biology are described in the
399 respective methods section.
400
401 **Aging and recording of lifespan**
402 100 flies (50 males and 50 females) were flipped onto fresh food every second day for up to 10
403 weeks. For lifespan recordings, flies were counted every other day or once a week. Please note
404 that conclusions regarding lifespan might be confounded by genetic background etc. as flies
405 have not been backcrossed for 10 generations or more. However, the lifespan experiments
406 were carried out solely to be able to correlate the lifespan of each group of flies to its respective
407 behavioral, physiological, or anatomical phenotype.
408
409 **Olfactory T-Maze assay**
410 1-10 weeks old flies collected on the same day were used for all experiments and tested on the
411 same day side by side. For experiments with RNAi, experimental flies and genetic controls were
412 raised at 30℃ to enhance the effect of the RNAi. Flies were tested in groups of ~60 (30 females
413 and 30 males) in a T-maze and were allowed 1 min to make a decision to go into either arm.
414 Experimentation was carried out within climate-controlled boxes at 25℃ and 60% rH in the
415 dark. 50 µl of fresh odor solution (all odors were purchased at Sigma-Aldrich) at different

416 concentrations diluted in distilled water or paraffin oil applied on Whatman chromatography
417 paper was provided in the odor tube, except for 1% CO_2, which was diluted using a custom-
418 build setup with mass flow controller from pure CO_2 and bottled air. Control tubes were filled
419 with 50 µl odorant solvent or compressed air in the case of CO_2. Unless otherwise indicated, 1
420 mM of odor dilution was used. After experimentation, the number of flies in each tube was
421 counted. An olfactory preference index (P.I.) was calculated by subtracting the number of flies
422 on the test odor site from the number of flies on the control site and normalizing by the total
423 number of flies. Statistical analysis was performed using ANOVA and the Bonferroni multiple
424 comparisons posthoc test using Prism GraphPad 6.
425
426 **Visual T-maze assay**
427 Experiments were essentially carried out as described above, but with a visual instead of an
428 olfactory stimulus. A modified transparent T-maze apparatus was used to allow stimulation with
429 light. The two arms of the T-maze were illuminated with blue LED emitting lights (465-470nm)
430 on one side or red LED lights (625-630 nm) on the other side. by subtracting the number of flies
431 on the test odor site from the number of flies on the control site and normalizing by the total
432 number of flies. Statistical analysis was performed using ANOVA and the Bonferroni multiple
433 comparisons posthoc test using Prism GraphPad 6.
434 In some experiments flies were videotracked by using an infrared camera on the top of the
435 climate box and analyzed with ctrax software.
436
437 **Treatment with *Lactobacillus plantarum* or *Acetobacter pomorum***
438 200 fly embryos (12 h AEL) were collected in a petri dish, washed with 10% bleach once, in
439 70% ethanol twice, in PBS once, and in sterile, distilled water twice. These embryos are
440 considered germfree and are referred to as *treated*. Embryos were then transferred into new

441 food bottles. An overnight *L. plantarum* culture was concentrated to OD:200 and 300 µl were
442 added into the fly food every third day.
443
444 **Treatment with Resveratrol**
445 For Resveratrol-supplemented diets, Resveratrol was dissolved in 100% ethanol and added to
446 fly food to a final concentration of 100 µM. All diets contained 1.5% agar and equal amounts of
447 ethanol.
448
449 **Anatomy**
450 Adult fly brains were dissected, fixed, and stained as described previously (Hartl et al., 2011).
451 Briefly, brains were dissected in cold PBS, fixed with paraformaldehyde (2%, overnight at 4℃ or
452 for 2 h at RT), washed in PBS, 0.1% Triton X-100, 10% donkey serum and stained overnight at
453 4° C or for 2 h at RT with the primary and after washes in PBS, 0.1% Triton X-100 with the
454 secondary antibody using the same conditions. All microscopic observations were made at an
455 Olympus FV-1000 or at a Leica SP8 confocal microscope. Images were processed using
456 ImageJ and Photoshop. The following antibodies were used: chicken anti-GFP and anti-RFP
457 (molecular probes, 1:100), rat anti-N-cadherin (anti-N-cad DN-Ex #8, Developmental Studies
458 Hybridoma Bank, 1:100), and mouse anti-ChAT (Yasuyama et al., 1995). Secondary antibodies
459 used were: anti-chicken Alexa 488 (molecular probes, 1:250), a-mouse Alexa 633 (molecular
460 probes, 1:250) and anti-rabbit Alexa 549 (molecular probes, 1:250), respectively.
461
462 For image quantification, all brains were processed at the same time using the same conditions.
463 Images were taken at the exact same settings. All analysis was done blind to the genotype or
464 age of the flies. For the quantification of cell bodies, neurons were counted section-by-section
465 either directly at the confocal or using ImageJ/FIJI software. For antibody staining or reporter
466 construct expression at the level of the lateral horn (LH), images were Z-projected into a single

467 image. Regions of interest (ROI) were drawn around the LH in each image and quantification
468 was carried out using FIJI ImageJ software. For quantification of stainings in the antennal lobe
469 (AL) and calyx, three sections at similar levels of the structures were chosen. ROIs were drawn
470 around the AL or calyx in each section and combined to quantify each individual brain. For each
471 brain, only one LH, calyx and AL were chosen randomly for quantifications. For quantification of
472 staining intensity, different strategies were used depending on the staining. For GCaMP
473 staining, all stainings were normalized to Ncad antibody staining. For Dα7-GFP and ToPro
474 staining, staining intensity was measured as mean grey value (MGV) and normalized to the size
475 of the area that was measured. For quantification of ChAT and mito-RFP staining in Figure 3,
476 ratios of stainings were calculated by dividing the MGV in the area of interest by another brain
477 area of equal size next to it, i.e. in a region of the brain just below the calyx that did not express
478 the protein or the reporter or that did not belong to the region of interest. With the aim to
479 calculate how brain areas were affected by aging relative to each other. A decrease in the ratio
480 showed that the MGV in for instance the calyx was more strongly decreased as compared to
481 another brain area. For Figure 5, ChAT staining was quantified as MGV. Measurements of cell
482 body size diameter were carried out in ImageJ/FIJI. 3 cell bodies were measured per section in
483 several sections of the brain or antenna. The averages of the measured diameters were used
484 for statistical analysis.
485 All statistical analysis was carried out with GraphPad Prism software. The exact statistics used
486 in each experiment are indicated in the respective figure legends. Of note, different absolute
487 values are the result of the use of two different confocal microscopes; the newer Leica SP8 was
488 significantly more sensitive as compared to the older Olympus FV1000. As the result, individual
489 settings for each microscope were used and absolute number can only be compared within
490 each individual graph.
491
492 ***Immunostaining for STED microscopy***

493 Brains were dissected in Ringer's solution (pH 7.3, 290 –310 mOsm) containing 5 mM HEPES-
494 NaOH, 130 mM NaCl, 5 mM KCl, 2 mM MgCl2, 2 mM CaCl2, and 36 mM sucrose, fixed in 4%
495 PFA for 2 h at 4℃ and washed three times for 10 min each in PBS containing 0.6% Triton X-
496 100 (PBT) at room temperature. Samples were incubated for 2 h in PBT containing 2% BSA
497 and 5% normal goat serum. Subsequently, the samples were incubated in the primary antibody
498 diluted in block solution at 4℃ overnight. For staining BRP-short^{GFP}, FluoTag-X4 anti-GFP,
499 Abberior Star 635P-conjugated (1:100, NanoTag Biotechnologies, N0304-Ab635P) and for
500 staining postsynaptic densities of Kenyon cells, rabbit anti-Drep- 2$^{C\text{-}Term}$ (1: 500, Andlauer et al.
501 2014) were used. Samples were washed three times for at least 30 min each in PBT containing
502 2% BSA (PAT) at room temperature, subsequently incubated with secondary antibody diluted in
503 PAT overnight at 4℃. As secondary antibody AlexaFluor-594-coupled goat anti-rabbit (1: 200,
504 Thermo Fisher Scientific, A-11012) was used. Brains were washed at least six times for 30 min
505 each in PBT and embedded in Prolong Gold Antifade (Invitrogen). Samples were stored for 24 h
506 at room temperature followed by 48 h at 4℃, before STED microscopy.
507
508 ***Two-Color STED imaging***
509 STED imaging with time-gated detection was performed on a Leica SP8 TCS STED microscope
510 (Leica Microsystems) equipped with a pulsed white light excitation laser (NKT Photonics). Dual-
511 channel STED imaging was performed by sequentially exciting Abberior Star 635P and Alexa
512 594 at 646 nm and 598 nm, respectively. Both dyes were depleted with a 775 nm STED laser.
513 Three optical sections at a distance of 250 nm were acquired with an HC PL APO CS2
514 100×/1.40-N.A. oil objective (Leica Microsystems), a scanning format of 1024 × 1024 pixel, 8 bit
515 sampling and 6 fold zoom, yielding a pixel dimension of 18.9 × 18.9 nm. Time-gated detection
516 was set from 0.3–6 ns for all dyes. To minimize thermal drift, the microscope was housed in a
517 heatable incubation chamber (LIS Life Imaging Services).
518

519 For quantifications, raw data obtained from STED imaging were de-convoluted using Huygens
520 Professional (Scientific Volume Imaging, Netherlands) and analyzed by a custom-written
521 ImageJ macro. Briefly, z-stacks of de-convoluted images were projected and each channel was
522 segmented using the auto local threshold method 'Phansalkar' followed by watershed
523 separation of touching segmented particles. The number, area fraction, and feret diameter from
524 all segmented particles with sizes from 5 to 200 pixels were measured in > 4 separate images
525 per calyx region.
526
527 ***In vivo* calcium imaging**
528 For calcium imaging experiments with an epifluorescence microscope, GCaMP3 was expressed
529 under the control of GH146-Gal4 (flies were heterozygous for both transgenes). Female flies
530 were prepared in a modified setup according to a method previously reported (Hussain et al.,
531 2016b). *In vivo* preparations were imaged using a Leica DM6000FS fluorescent microscope
532 equipped with a 40x water immersion objective and a Leica DFC360 FX fluorescent camera. All
533 images were acquired with the Leica LAS AF E6000 image acquisition suit. Images were
534 acquired for 20 s at a rate of 20 frames per second with 4 x 4 binning mode. To calculate the
535 normalized change in the relative fluorescence intensity, we used the following formula: $\Delta F/F =$
536 $100(Fn-F0)/F0$, where Fn is the nth frame after stimulation and F0 is the averaged basal
537 fluorescence of 15 frames before stimulation. The peak fluorescence intensity change is
538 calculated as the mean of normalized trace over a 2 s time window during the stimulation
539 period. During all measurements, the exposure time was kept constant at 20 ms. For all
540 experiments with odor stimulation, the stimulus was applied 5 s after the start of each
541 measurement. A continuous and humidified airstream (2000 ml/min) was delivered to the fly
542 throughout the experiment via an 8 mm diameter glass tube positioned 10 mm away from the
543 preparation. A custom-made odor delivery system (Smartec, Martinsried), consisting of mass
544 flow controllers (MFC) and solenoid valves, was used for delivering a continuous airstream and

545 stimuli in all experiments. In all experiments, stimuli were delivered for 500 ms, and during
546 stimulations the continuous flow was maintained at 2,000 ml/min. For odorant stimulations, 1 ml
547 of a precise concentration was filled in the odor delivery cup and the collected airspace odor
548 was injected into the main airstream to give 0 mM, 0.1mM, 1mM, and 10mM final concentrations
549 for 500 ms without changing airstream strength. To measure the fluorescent intensity change,
550 the region of interest was delineated by hand and the resulting time trace was used for further
551 analysis. To calculate the normalized change in the relative fluorescence intensity, we used the
552 following formula: $\Delta F/F = 100(FnF0)/F0$, where Fn is the nth frame after stimulation and F0 is
553 the averaged basal fluorescence of 15 frames before stimulation. The peak fluorescence
554 intensity change is calculated as the mean of normalized trace over a 2 s time window during
555 the stimulation period. The pseudo-colored images were generated in MATLAB using a custom
556 written program. All analysis and statistical tests were done using Excel and GraphPad6 Prism
557 software, respectively.
558 For live imaging using two-photon microscopy, flies were homozygous for both GH146-Gal4 and
559 the UAS-GCaMP3 construct. Female transgenic flies (5–6 day, 4 week and 6 weeks old) were
560 used for imaging experiments. Imaging was performed using two-photon microscope (Leica)
561 equipped with a 20x water-immersion objective (NA=1, Leica). GCaMP3 was excited at 920 nm.
562 A custom-built device was used as odor delivery system to supply odors with a constant flow
563 rate of 1 ml/s to the fly's antennae for 2 sec. Onset and duration of the odor stimulus were
564 controlled using a custom-written LABVIEW program. Images were recorded at 5 Hz. Image
565 processing and analysis was performed using Fiji software. For correcting the potential slight
566 movements in x-y direction, recorded images were aligned using TurboReg plugin (Thevenaz et
567 al., 1998). Afterwards, regions of interest (ROIs) were manually defined. In the antennal lobe,
568 individual glomeruli and in the calyx, individual presynaptic boutons were selected as ROIs. For
569 signal quantification, the average pixel intensity of five frames before stimulus onset was

570 determined as F. ΔF is the difference between fluorescence and F, and resulting values were
571 divided by F and displayed as percent.
572
573 ***In vivo* electrophysiology**
574 Single sensillum recordings (SSR) are extracellular recordings performed from antennal
575 olfactory sensilla as previously described (Hartl et al., 2011). A single fly was wedged into
576 narrow end of a truncated 200 µl pipette tip and placed on a slide under the objective. The fly
577 head was exposed and stabilized on top of a glass coverslip. The antennae were hold by the tip
578 of a glass capillary. An odor delivery pipette blew continuous air-streams to the antenna
579 providing odor stimulations of different concentrations (SYNTECH, the Netherlands). A glass
580 reference electrode filled with ringer (0.01 mM KCl) was inserted into the fly eye gently by a
581 micromanipulator (Sutter instruments). And a glass recording electrode filled with ringer (0.01
582 mM KCl) was pushed against a sensillum until it pierced the cuticular wall of the sensillum. The
583 recording of action potentials (APs) was started after an observation of spontaneous responses
584 of olfactory neurons. The AC signals (10 -2800 Hz) of the responses were amplified 500x
585 (Multiclamp 700B, United States) and were analyzed with Clampex10.3 software (Digidata
586 1440A, the United States). The signals to a particular stimulus were recorded 5 seconds before
587 giving the odor stimulation. The responses of neurons were calculated by counting the number
588 of APs for 0.5s during the response minus the number of APs for 0.5s before the response
589 (spikes/s). Statistical analysis was performed by one-way ANOVA using GraphPad Prism
590 software.
591
592 **RNA-sequencing**
593 RNA was extracted and sequencing was carried out using standard methods and as previously
594 described (Hussain et al., 2016a). RNA-sequencing was performed using the Illumina HiSeq
595 2000/2500 sequencer suite.

596

597 ***Statistical methods for RNA-seq and gene ontology analysis***

598 Gene expression data was normalized by size factors and tested for differential expression
599 using DESeq2 package (v. 1.16.1) (Love et al., 2014)in R (v. 3.4.0). Significant up and down
600 regulated genes were classified according to their $\log_2$ fold change and adjusted p-value < 0.01.
601 Then, up and down regulated genes were analyzed separately to obtain enriched gene ontology
602 terms using topGO package (v. 2.28.0) in R and the *D. melanogaster* gene ontology annotation
603 database gene_association.fb (http://www.flybase.org).

604

605 **References**

606

607 Andlauer, T.F., Scholz-Kornehl, S., Tian, R., Kirchner, M., Babikir, H.A., Depner, H., Loll, B., Quentin, C.,
608 Gupta, V.K., Holt, M.G.*, et al.* (2014). Drep-2 is a novel synaptic protein important for learning and
609 memory. Elife *3*.
610 Canter, R.G., Penney, J., and Tsai, L.H. (2016). The road to restoring neural circuits for the treatment of
611 Alzheimer's disease. Nature *539*, 187-196.
612 Christiansen, F., Zube, C., Andlauer, T.F., Wichmann, C., Fouquet, W., Owald, D., Mertel, S., Leiss, F.,
613 Tavosanis, G., Luna, A.J.*, et al.* (2011). Presynapses in Kenyon cell dendrites in the mushroom body
614 calyx of Drosophila. J Neurosci *31*, 9696-9707.
615 Court, F.A., and Coleman, M.P. (2012). Mitochondria as a central sensor for axonal degenerative stimuli.
616 Trends Neurosci *35*, 364-372.
617 Doty, R.L. (2012). Olfaction in Parkinson's disease and related disorders. Neurobiol Dis *46*, 527-552.
618 Doty, R.L., Shaman, P., Applebaum, S.L., Giberson, R., Siksorski, L., and Rosenberg, L. (1984). Smell
619 identification ability: changes with age. Science *226*, 1441-1443.
620 Fukui, M., Choi, H.J., and Zhu, B.T. (2010). Mechanism for the protective effect of resveratrol against
621 oxidative stress-induced neuronal death. Free Radic Biol Med *49*, 800-813.
622 Granzotto, A., and Zatta, P. (2014). Resveratrol and Alzheimer's disease: message in a bottle on red wine
623 and cognition. Front Aging Neurosci *6*, 95.
624 Hartl, M., Loschek, L.F., Stephan, D., Siju, K.P., Knappmeyer, C., and Kadow, I.C. (2011). A new
625 Prospero and microRNA-279 pathway restricts CO2 receptor neuron formation. J Neurosci *31*, 15660-
626 15673.
627 Humphrey, D.M., Parsons, R.B., Ludlow, Z.N., Riemensperger, T., Esposito, G., Verstreken, P., Jacobs,
628 H.T., Birman, S., and Hirth, F. (2012). Alternative oxidase rescues mitochondria-mediated dopaminergic
629 cell loss in Drosophila. Hum Mol Genet *21*, 2698-2712.
630 Hussain, A., Ucpunar, H.K., Zhang, M., Loschek, L.F., and Grunwald Kadow, I.C. (2016a). Neuropeptides
631 Modulate Female Chemosensory Processing upon Mating in Drosophila. PLoS Biol *14*, e1002455.
632 Hussain, A., Zhang, M., Ucpunar, H.K., Svensson, T., Quillery, E., Gompel, N., Ignell, R., and Grunwald
633 Kadow, I.C. (2016b). Ionotropic Chemosensory Receptors Mediate the Taste and Smell of Polyamines.
634 PLoS Biol *14*, e1002454.
635 Juhasz, G., Erdi, B., Sass, M., and Neufeld, T.P. (2007). Atg7-dependent autophagy promotes neuronal
636 health, stress tolerance, and longevity but is dispensable for metamorphosis in Drosophila. Genes Dev
637 *21*, 3061-3066.
638 Kirby, K., Hu, J., Hilliker, A.J., and Phillips, J.P. (2002). RNA interference-mediated silencing of Sod2 in
639 Drosophila leads to early adult-onset mortality and elevated endogenous oxidative stress. Proc Natl Acad
640 Sci U S A *99*, 16162-16167.

641 Kittel, R.J., Wichmann, C., Rasse, T.M., Fouquet, W., Schmidt, M., Schmid, A., Wagh, D.A., Pawlu, C.,
642 Kellner, R.R., Willig, K.I.*, et al.* (2006). Bruchpilot promotes active zone assembly, Ca2+ channel
643 clustering, and vesicle release. Science *312*, 1051-1054.
644 Kong, F., Hua, Y., Zeng, B., Ning, R., Li, Y., and Zhao, J. (2016). Gut microbiota signatures of longevity.
645 Curr Biol *26*, R832-833.
646 Kremer, M.C., Christiansen, F., Leiss, F., Paehler, M., Knapek, S., Andlauer, T.F., Forstner, F.,
647 Kloppenburg, P., Sigrist, S.J., and Tavosanis, G. (2010). Structural long-term changes at mushroom body
648 input synapses. Curr Biol *20*, 1938-1944.
649 Kurowska, Z., Kordower, J.H., Stoessl, A.J., Burke, R.E., Brundin, P., Yue, Z., Brady, S.T., Milbrandt, J.,
650 Trapp, B.D., Sherer, T.B.*, et al.* (2016). Is Axonal Degeneration a Key Early Event in Parkinson's
651 Disease? J Parkinsons Dis *6*, 703-707.
652 Leinwand, S.G., Yang, C.J., Bazopoulou, D., Chronis, N., Srinivasan, J., and Chalasani, S.H. (2015).
653 Circuit mechanisms encoding odors and driving aging-associated behavioral declines in Caenorhabditis
654 elegans. Elife *4*, e10181.
655 Lopez-Otin, C., Blasco, M.A., Partridge, L., Serrano, M., and Kroemer, G. (2013). The hallmarks of aging.
656 Cell *153*, 1194-1217.
657 Love, M.I., Huber, W., and Anders, S. (2014). Moderated estimation of fold change and dispersion for
658 RNA-seq data with DESeq2. Genome Biol *15*, 550.
659 MacDermott, A.B., Role, L.W., and Siegelbaum, S.A. (1999). Presynaptic ionotropic receptors and the
660 control of transmitter release. Annu Rev Neurosci *22*, 443-485.
661 Massaad, C.A., Washington, T.M., Pautler, R.G., and Klann, E. (2009). Overexpression of SOD-2
662 reduces hippocampal superoxide and prevents memory deficits in a mouse model of Alzheimer's disease.
663 Proc Natl Acad Sci U S A *106*, 13576-13581.
664 Oka, S., Hirai, J., Yasukawa, T., Nakahara, Y., and Inoue, Y.H. (2015). A correlation of reactive oxygen
665 species accumulation by depletion of superoxide dismutases with age-dependent impairment in the
666 nervous system and muscles of Drosophila adults. Biogerontology *16*, 485-501.
667 Pircs, K., Nagy, P., Varga, A., Venkei, Z., Erdi, B., Hegedus, K., and Juhasz, G. (2012). Advantages and
668 limitations of different p62-based assays for estimating autophagic activity in Drosophila. PLoS One *7*,
669 e44214.
670 Sama ul, H., Tahir, M., and Lone, K.P. (2008). Age and gender-related differences in mitral cells of
671 olfactory bulb. J Coll Physicians Surg Pak *18*, 669-673.
672 Scheperjans, F., Aho, V., Pereira, P.A., Koskinen, K., Paulin, L., Pekkonen, E., Haapaniemi, E.,
673 Kaakkola, S., Eerola-Rautio, J., Pohja, M.*, et al.* (2015). Gut microbiota are related to Parkinson's disease
674 and clinical phenotype. Mov Disord *30*, 350-358.
675 Schwarzer, M., Makki, K., Storelli, G., Machuca-Gayet, I., Srutkova, D., Hermanova, P., Martino, M.E.,
676 Balmand, S., Hudcovic, T., Heddi, A.*, et al.* (2016). Lactobacillus plantarum strain maintains growth of
677 infant mice during chronic undernutrition. Science *351*, 854-857.
678 Seeley, W.W. (2017). Mapping Neurodegenerative Disease Onset and Progression. Cold Spring Harb
679 Perspect Biol *9*.
680 Storelli, G., Defaye, A., Erkosar, B., Hols, P., Royet, J., and Leulier, F. (2011). Lactobacillus plantarum
681 promotes Drosophila systemic growth by modulating hormonal signals through TOR-dependent nutrient
682 sensing. Cell Metab *14*, 403-414.
683 Tang, W., Xing, Z., Hu, W., Li, C., Wang, J., and Wang, Y. (2016). Antioxidative effects in vivo and
684 colonization of Lactobacillus plantarum MA2 in the murine intestinal tract. Appl Microbiol Biotechnol *100*,
685 7193-7202.
686 Thevenaz, P., Ruttimann, U.E., and Unser, M. (1998). A pyramid approach to subpixel registration based
687 on intensity. IEEE Trans Image Process *7*, 27-41.
688 Vagnoni, A., and Bullock, S.L. (2016). A simple method for imaging axonal transport in aging neurons
689 using the adult Drosophila wing. Nat Protoc *11*, 1711-1723.
690 Vaiserman, A.M., and Marotta, F. (2016). Longevity-Promoting Pharmaceuticals: Is it a Time for
691 Implementation? Trends Pharmacol Sci *37*, 331-333.
692 Valadas, J.S., Vos, M., and Verstreken, P. (2015). Therapeutic strategies in Parkinson's disease: what we
693 have learned from animal models. Ann N Y Acad Sci *1338*, 16-37.
694 Willig, K.I., Kellner, R.R., Medda, R., Hein, B., Jakobs, S., and Hell, S.W. (2006). Nanoscale resolution in
695 GFP-based microscopy. Nat Methods *3*, 721-723.

696 Wilson, R.I. (2013). Early olfactory processing in Drosophila: mechanisms and principles. Annu Rev
697 Neurosci *36*, 217-241.
698 Wood, J.G., Rogina, B., Lavu, S., Howitz, K., Helfand, S.L., Tatar, M., and Sinclair, D. (2004). Sirtuin
699 activators mimic caloric restriction and delay ageing in metazoans. Nature *430*, 686-689.
700 Yasuyama, K., Kitamoto, T., and Salvaterra, P.M. (1995). Localization of choline acetyltransferase-
701 expressing neurons in the larval visual system of Drosophila melanogaster. Cell Tissue Res *282*, 193-
702 202.
703

704 **Figure legends**

705

706 **Figure 1. The sense of smell ages faster than the sense of vision**. (A) Olfactory preference
707 index of aging Canton S flies to aversive (benzaldehyde, 3-octanol) and attractive odors (2,3-
708 butanedione, putrescine) in the T-maze assay. There is a gradual and significant ($p \leq 0.01$)
709 decrease in olfactory preference with aging (1 – 10 weeks). For additional odors see Figure S1.
710 (B) Preference index (X-axis) of flies to blue light versus red light in the T-maze assay against
711 age (Y-axis). There was no significant difference between the data points. Graphs show mean
712 value ± SEM (n = 8 trials, 60 flies/trial 30 ♀ and 30 ♂). (C) Schematic illustration of the fly brain
713 and antennal appendages with olfactory sensory neurons (OSNs). OSNs project into the
714 antennal lobe (AL), where they innervate a specific glomerulus (green). Projection neurons
715 (PNs, blue) send the information mainly to two higher brain centres, the mushroom body (MB)
716 and the lateral horn (LH) (top).

717

718 **Figure 2. Cholinergic projection neurons functionally decay with age**. (A) Scheme of in
719 vivo functional imaging preparation. The Ca2+ sensor GCaMP3 is expressed in projection
720 neurons (PNs) under the control of GH146-Gal4 (*GH146-Gal4;UAS-GCaMP3* or
721 GH146>GCaMP). (B_{1-3}) *In vivo* calcium imaging in PNs (*GH146-Gal4;UAS-GCaMP3.0*) at the
722 level of the AL using epifluorescence microscopy. The neural response of 1 week and 7 weeks
723 old flies to increasing concentrations of benzaldehyde, 2,3-butanedione and 3-octanol was
724 compared (n=8 ± SEM). Graphs represent the quantification of neural peak ΔF responses (in
725 %ΔF/F) in the strongest responding glomeruli to different concentrations of odors for 1 week
726 and 7 weeks old flies (n=8 ± SEM). All GCaMP3-fluorescence responses were calculated in
727 %ΔF/F. All p-values were calculated via Student's t-test (ns > 0.05, *$p \leq 0.05$, **$p \leq 0.01$). (C,
728 C´) GCaMP fluorescence changes are recorded in three different responsive glomeruli (DC2,
729 DM6 and DP1) upon stimulation with 3-octanol (12 mM). (D-D´) GCaMP fluorescence changes

730 were measured in three responsive glomeruli (DC1, DP1 und VC2) upon stimulation with 4-
731 methylcyclohexanol (16 mM) in 1, 4 and 6 weeks old flies. (C, D) Maximum fluorescence
732 changes of GCaMP3 upon odor stimulation in three different glomeruli. Scale bars: 20 µm. (C´,
733 D´) Odor-induced fluorescence change of GCaMP3 is indicated as false color images (top row)
734 for one representative animal. Fluorescence changes over time are shown in the lower row for
735 each different glomerulus. The pink bars represent the time window of odor presentation. n=9;
736 one-way ANOVA with *post hoc* Bonferroni tests. ns, not significant ($p > 0.05$). *$p < 0.05$. **$p <$
737 0.01. ***$p < 0.001$. (E-G) Expression of the Ca2+ sensor GCaMP3 in PNs under the control of
738 GH146-Gal4 visualized in two focal planes in presynaptic boutons of projection neurons in
739 calyces. Scale bars: 20 µm. (E) Representative image of *in vivo* two-photon imaging of
740 fluorescence of GCaMP3 in PNs (GH146>GCaMP) at their axonal extensions (boutons) in the
741 mushroom body calyx is shown in top image. Odor-induced fluorescence change of GCaMP3
742 are indicated as false color images (bottom image) for one representative animal. (F) Maximal
743 fluorescence changes of GCaMP3 in individual responsive boutons and (G) number of
744 responsive boutons upon stimulation with 3-octanol (12 mM), 4-methylcyclohexanol (16 mM) or
745 linalool (11 mM) in the two imaged focal planes. n= 9-11; one-way ANOVA with *post hoc*
746 Bonferroni tests. ns, not significant ($p > 0.05$). *$p < 0.05$. **$p < 0.01$. ***$p < 0.001$. All traces
747 represent mean ± SEM of ΔF/F values. Box plots indicate means, medians, interquartile ranges,
748 and 1 – 99 % ranges.
749
750 **Figure 3. Changes in axon and synapse integrity could affect projection neuron function**.
751 (A) Projection neurons (PNs) of a 1 and a 7 weeks old brains are labeled with a reporter line
752 (*GH146-Gal4;UASGCaMP3* or *GH146>GCaMP3*) and stained with an anti-GFP antibody
753 (green). AL, antennal lobe; cx, mushroom body calyx; LH, lateral horn; lateral cell body cluster is
754 shown in dotted box. Scale bar: 25 µm. (B) Average number of PNs in the lateral, dorsal
755 clusters and the total of both clusters. Orange boxes represent young flies (1 week), while grey

756 boxes represent old flies (7 weeks) in all figures. There is a mild but significant decrease in the
757 number of reporter-labeled PNs in aged flies (Students t-test, n = 19-21) (C) Average diameter
758 of projection neuron cell body sizes of 1 (orange) and 7 (grey) weeks old flies. The cell bodies of
759 PNs of aged flies are significantly smaller (Students t-test, n = 19-21). (D) The box plot shows
760 that there is no change in the expression of NCad in the defined areas for quantification
761 (antibody staining against N-cadherin as a synaptic marker) in 1 (orange) and 7 (grey) weeks
762 old flies AL and LH (Students t-test, n = 19-21). (E) Normalized expression levels of the GCaMP
763 reporter protein in PNs (*GH146>GCaMP3)* in young and old flies. The expression was
764 normalized to Ncad antibody staining. There is no reduction of GCaMP expression in old as
765 compared to young flies, but instead a slight but significant increase (Students t-test, n = 19-21).
766 (F) Volcano plot of RNA-sequencing data of selected genes displaying the genes that are
767 downregulated and upregulated in 7 weeks old brains compared to 1 week old brains,
768 respectively. Only genes above the cutoff of –log10 (p-value adjusted (padj)) are considered
769 significantly changed (above black line). While several AChR receptors were significantly
770 downregulated in the brain, this was not the case in the antenna (Figure 4 – Figure Supplement
771 2C). In addition, several aging-related genes are upregulated in older brains. Selected genes
772 are displayed and were color-labeled by gene ontology analysis (orange: aging; green: neuronal
773 function). (G) Reporter construct showing the localization of acetylcholine receptor (AChR) Dα7
774 (*GH146-Gal4;UAS-Dα7-GFP*, stained with anti-GFP antibody (green)) and ToPro nuclear
775 marker (shown in pink) in the AL and lateral horn (LH). There is a decline at PN postsynaptic
776 sites in the AL supporting an aging-related decline in the integrity of cholinergic synapses. For
777 instance, the localization of Dα7 at presynaptic terminals and axons is lost in old flies (n=20/20)
778 in contrast to young animals (n=0/20). See missing signal in axon and presynaptic terminals in
779 the MB calyx and LH. Scale bar: 25 µm (H) Quantification of mean gray value (MGV) of ToPro
780 staining of cell bodies in the area of the LH revealed a decrease in the number of cells in old as

781 compared to young flies (n=20). (I) A box plot shows a significant reduction in the AChR Dα7
782 reporter construct signal (mean grey value, MGV) of 7 weeks old flies (grey) compared to 1
783 week old flies (orange) at the level of the AL. Box plots show median and upper/lower quartiles.
784 All p-values represent: ns > 0.05, *p ≤ 0.05, **p ≤ 0.01, ***p ≤ 0.001. (J) Representative images
785 of antennal lobes of 1 and 7 weeks old flies. Brains express the reporter mito-mcherry in PNs
786 (*GH146-Gal4;UAS-mito-mcherry;* anti-RFP, red) and are stained for anti-ChAT (blue). (K)
787 Representative images of the mushroom body calyx of 1 and 7 weeks old flies. (L)
788 Quantification of relative expression of a mitochondria reporter (*GH146-Gal4;UAS-mito-*
789 *mcherry*) and ChAT in AL, LH, and calyx. Note that mitochondria and ChAT staining are
790 significantly reduced in the MB calyx as compared to an mito-mcherry or ChAT expression in
791 other parts of the brain in old flies as compared to younger animals (see methods). This
792 suggests that ChAT does not decrease equally in all brain parts, but in particular in areas such
793 as the MB calyx. Graphs display mean relative levels ±SEM. Student's t-test: ns > 0.05, *p ≤
794 0.05, **p ≤ 0.01, ***p ≤ 0.001. (M) Confocal and high-resolution STED microscopy images in the
795 calyx of flies expressing BRP-short^{GFP} under control of GH146-Gal4 driver line. Green and
796 magenta represent anti-GFP and anti-Drep2$^{C\text{-}Term}$ immunostaining, respectively. White squares
797 in (M, left column) indicate the magnified region in (M, right column). Scale bars represent 2 μm
798 in (M, left) and 0.5 μm in (M, right). (N) Number of active zones and (O) postsynaptic densities
799 significantly decrease upon aging. n= 10-12; Student's t-test. ***p < 0.001. Box plots indicate
800 means, medians, interquartile ranges, and 1-99 % ranges.
801
802 **Figure 4. Superoxide dismutase 2 is selectively required in projection neurons**. (A) RNAi
803 knockdown behavioral screening of selected candidate genes involved in systemic aging, in the
804 T-maze assay. RNAi Knockdown of *SOD2* (superoxide dismutase 2) pan-neuronally using the
805 line elav-Gal4 (*elav>SOD2i*) in 3 weeks old flies significantly reduced olfactory attraction to 2,3
806 butanedione. In addition, two mutants (3 weeks of age) of autophagy genes did not show a

807 defect in olfactory preference behavior (see Figure 4 – Figure Supplement 1A) (B) RNAi knock-
808 down of SOD2 in OSNs had no effect on the flies' olfactory preference suggesting that OSNs
809 might be less sensitive to oxidative stress. Box plots show olfactory PIs of 1 week old flies
810 expressing an RNAi knock-down construct for SOD2 under the control of *ORCO*, which is
811 expressed broadly in OSNs *(ORCO-Gal4;UAS-SOD2-RNAi)* and their genetic controls to 2,3-
812 butanedione, benzaldehyde and 3-octanol in the T-maze assay. (C) RNAi knock-down of SOD2
813 in PNs using the GH146-Gal4 *(GH146-Gal4;UAS-SOD2-RNAi)*, results in strongly diminished
814 olfactory preference of flies to 2,3-butanedione, benzaldehyde and 3-octanol. Box plots show
815 median and upper/lower quartiles (n = 8, 60 flies/trial, 30 ♀ and 30 ♂). All p-values were
816 calculated via one-way ANOVA with the Bonferroni multiple comparison posthoc test (ns > 0.05,
817 *p ≤ 0.05, **p ≤ 0.01, ***p ≤ 0.001).
818
819 **Figure 5. SOD2 deprived PNs resemble neurons in aged brains**
820 (A) SOD2 RNAi (*GH146-Gal4;UAS-SOD2i*) expressing and SOD2 RNAi negative controls
821 labeled with the reporter line (*GH146-Gal4;UASGCaMP3* or *GH146>GCaMP3*) and stained with
822 an anti-GFP antibody (green). AL, antennal lobe; cx, mushroom body calyx; LH, lateral horn;
823 lateral cell body cluster is shown in dotted box. Scale bar: 25 µm. (B) Average number of PNs in
824 the lateral, dorsal clusters and the total of both clusters. Orange boxes represent 1 week control
825 flies, while blue boxes represent flies carrying GH146>SOD2i in all figures. There is no
826 significant decrease in the number of reporter-labeled PNs upon SOD2 knock-down (Students t-
827 test, n = 19-21) (C) Average diameter of projection neuron cell body sizes of controls (orange)
828 and SOD2 knock-down flies (blue). The cell bodies of PNs are significantly smaller when SOD2
829 is reduced exclusively in PNs (Student's t-test, n=19-21). (D) Scatter plots showing normalized
830 GCaMP signal stained with α-GFP antibody (MGV). The intensity of staining within the LH
831 (upper panel) and within the calyx (bottom panel) was normalized to the background signal in a
832 non-GFP positive brain area of the same brain (Student's t-test, n=28). (E) Mean gray value

833 (MGV) of anti-ChAT antibody staining in the MB calyx. Note that knocking-down SOD2 in PNs
834 significantly reduced the ChAT signal (Student's t-test, n=28). (F) Representative image of *in*
835 *vivo* two-photon imaging of fluorescence of GCaMP3 in PNs (GH146>GCaMP) at their axonal
836 extensions (boutons) in the mushroom body calyx for test (*GH146>GCaMP;SOD2i*) and control
837 flies (*GH146>GCaMP;+*). Odor-induced fluorescence change of GCaMP3 are indicated as false
838 color images (right column) for one representative animal of each genotype. Scale bars: 20 µm.
839 (G) maximal fluorescence changes of GCaMP3 in individual responsive boutons and (H)
840 number of responsive boutons upon stimulation with 3-octanol (12 mM) or 4-methylcyclohexanol
841 (16 mM) in the two imaged focal planes. n= 10; Student's t-test. (ns > 0.05, *p ≤ 0.05, **p ≤
842 0.01, ***p ≤ 0.001). Box plots indicate means, medians, interquartile ranges, and 1-99 %
843 ranges.
844
845 **Figure 6. Expression of SOD2 in single neuron subtype fully rescues olfactory**
846 **degeneration**. (A) Box plots show PIs of 1 week old (orange boxes) and 7 weeks old (grey
847 boxes) transgenic flies overexpressing SOD2 exclusively in projection neurons (PNs) *(GH146-*
848 *Gal4;UAS-SOD2)* and their genetic controls in response to attractive (2,3-butanedione) and
849 aversive (3-octanol) odors. Note that expression of SOD2 exclusively in PNs fully rescues
850 olfactory performance in 7 weeks old flies indicating that sensitivity to oxidative stress of PNs
851 represents a key player in the aging-associated decline of the olfactory system. (B) Box plots
852 show PIs of 1 week old (orange) and 7 weeks old (grey) transgenic flies overexpressing SOD2
853 under the control of *ORCO-Gal4* in OSNs *(ORCO-Gal4;UAS-SOD2)* and their genetic controls
854 in response to attractive (2,3-butanedione) and aversive (3-octanol) odors. Importantly,
855 overexpression of SOD2 under the control of *ORCO-Gal4* in OSNs had no effect on the
856 behavior of old flies. (C) Box plots show preference of 1 week old and 7 weeks old flies raised
857 on standard fly food (first 2 boxes) and 7 weeks old flies raised on standard fly food mixed with
858 Resveratrol (third grey box) in response to attractive (2,3-butanedione) and aversive (3-octanol)

odors. All p-values were calculated via t-test (ns > 0.05, *p ≤ 0.05, **p ≤ 0.01, ***p ≤ 0.001). In all figures, asterisks above a single bar refer to p-values of comparison to the control (7 weeks old flies in 2nd bar). (D) Box plots show untreated and treated (flies were inoculated with the indicated bacterial strain after being pretreated to become germfree) 1 week old (light (treated) and dark orange (not germfree, standard conditions as in all other experiments before) and 7 weeks old (dark and light grey) flies. Treated flies were inoculated with *Lactobacillus plantarum NI202877, L. plantarum WJL, Acetobacter pomorum (A.p.),* while control flies were just raised on standard fly food. P.I.s of flies to the attractive odor 2,3-butanedione is shown. All p-values were calculated via two-way ANOVA with the Bonferroni multiple comparison posthoc test (ns > 0.05, *p ≤ 0.05, **p ≤ 0.01, ***p ≤ 0.001). Asterisks above a single box refer to p-values of comparison to the control (7 weeks old treated control). Box plot show median and upper/lower quartiles (n = 8, 60 flies/trial 30 ♀ and 30 ♂). (E) Summary and model of presented results. SOD2, the mitochondrial form of SOD, protects projection neurons (PN) from oxidative stress. Their vulnerability to oxidative stress and reactive oxygen species (ROS) appears to be the weak point of the olfactory system of Drosophila. The decline in function of PNs ultimately results in strongly reduced sensitivity to odors and accordingly diminishes behavioural responses.

879 **Supplementary figures and figure legends**

880

881 **Figure 1 – Figure Supplement 1.** (A-D) Olfactory preference index of the aging Canton S flies
882 to attractive (pentanoic acid) and aversive odors (4-methyl cyclohexanol, Linalool, CO_2) in the T-
883 maze assay. Y-axis indicates the preference index (P.I.) to odors while X-axis denotes age
884 (weeks) of the tested flies. (E-G) Aging affects all classes of OSNs. Olfactory preference index
885 of the odorant receptor co-receptor *ORCO mutant* aging flies in the T-maze assay in response
886 to 3 attractive odors (pentanoic acid, putrescine, 2-3 butanedione). Y-axis indicates the
887 preference index (P.I.s) to odors while X-axis denotes age (weeks) of the tested flies. Flies
888 show response to putrescine (F), because it is detected by ionotropic receptors class (IR41a)
889 instead of olfactory receptors (Hussain et al., 2016). (H-L) Olfactory preference index of the
890 aging Canton S flies in the T-maze assay in response to 5 aversive odors (Benzaldehyde, 4
891 methyl cyclohexanol, 3-octanol, Linalool, and CO_2). Flies show response to CO_2 (L), because it
892 is detected by gustatory receptors (Gr21a, Gr63a) (Jones et al., 2007) instead of olfactory
893 receptors. Box plot shows median and upper/lower quartiles (n = 8, 60 flies/trial 30 ♀ and 30 ♂).
894 All p-values were calculated via two-way ANOVA with the Bonferroni multiple comparison
895 posthoc test (ns > 0.05, *p ≤ 0.05, **p ≤ 0.01, ***p ≤ 0.001).

896

897 **Figure 2 - Figure Supplement 1.** (A) Expression of a reporter construct for specific olfactory
898 sensory neurons (OSN) in 1-10 weeks old flies with a transgenic reporter construct (*Or42b-*
899 *Gal4;UAS-mCD8GFP*). Scale bars: 15 µm. Box plot shows median and upper/lower quartiles for
900 the number of OR42b neurons in 1-10 weeks old flies. No difference in OSN number was
901 detected between young (1 week) and older flies (10 weeks). P-value was calculated via one-
902 way ANOVA (ns > 0.05, *p ≤ 0.05, **p ≤ 0.01, ***p ≤ 0.001). (B) The size of OSN cell bodies did
903 not change during aging (OR42b>mCD8GFP labeled cell bodies of 1 week *vs.* 10 weeks old
904 flies; N = 20 flies per group, n = 71 and 72 neurons). P-value was calculated using Standard t-

905 test. (C) Number of all ORs, IRs, and GRs upregulated and downregulated (non-significantly) in
906 7 weeks old fly antenna during aging. In addition, some receptors remained unchanged
907 between the two conditions. (D) Volcano plot of RNA-sequencing data of selected olfactory
908 receptor genes displaying the receptors that are involved in recognition of the tested odorants.
909 Only genes above the cutoff of –log10 (p-value adjusted (padj)) are considered significantly
910 changed. (E) Scatter plot displaying the correlation of gene expression between samples from 1
911 and 7 weeks old brains. The high correlation indicates that the majority of genes in the brain
912 remains unchanged, while a smaller number of genes change their expression.
913
914 **Figure 2 - Figure Supplement 2.** (A) Schematic illustration of the electrophysiology setup. (B-
915 H) Neural activity of olfactory sensory neurons (OSNs) in electrophysiological single sensilum
916 recordings (SSR) in response to 10 mM of attractive (2,3-butanedione, hexanoic acid, 1-
917 propanol) and aversive (acetophenone,1-octen-3-ol, Benzaldehyde, CO_2, 3-octanol) odors. The
918 responses were compared between 1 week and 5 weeks old flies (n=8 ± SEM). Each graph
919 shows responses (spike/sec) on Y-axis while the X-axis indicates the age (weeks) of the flies.
920 (n=8). Sample response traces are displayed on the right side of each graph. (J) Neural activity
921 response (spike/sec) of young (1 week) and old (7 week) flies that show normal aversion
922 (responders) and no aversion (non-responders) in T-maze assay, to aversive odor 3-octanol.
923 The flies were sorted by behavioral performances before the SSR experiments. Responders
924 were flies that showed the expected young fly behavioural response to an odor, while non-
925 responder flies did not respond to an odor as expected in the olfactory behaviour assay. Y-axis
926 shows neural response (spike/sec) whereas X-axis indicates the concentration of the odor
927 (n=8). (K) Neural activity response (spike/sec) of young (1 week) and old (7 week) flies that
928 show normal attraction (responders) and no attraction (non-responders) in the T-maze assay, to
929 attractive odor 2,3-butanedione. Y-axis shows neural responses (spike/sec), whereas the X-axis

930 indicates the concentration of the odor (n=8). These data suggest that behavioral changes do
931 not correlate with responses of OSNs to odors.
932
933 **Figure 2 - Figure Supplement 3**. Schematic illustration of the T-maze olfactory assay.
934 Olfactory preference index of the 1 week (orange) and 7 weeks (grey) old wildtype (Canton S)
935 flies to standard 1 mM and increased 10 mM attractive (2,3-butanedione, putrescine) and
936 aversive (benzaldehyde, 3-octanol) odors in the T-maze assay. Y-axis indicates the preference
937 index (P.I.) to odors, while the X-axis denotes concentration of the tested odors. Note that the
938 increase in odor concentration strongly improves the flies' performance in the test suggesting
939 that flies suffer from decreased sensitivity but not from failure to recognize and evaluate the
940 odor. Box plot show median and upper/lower quartiles (n = 8, 60 flies/trial 30 ♀ and 30 ♂).
941
942 **Figure 4 - Figure Supplement 1.** (A) Olfactory preference index of two different autophagy
943 gene mutant (*atg*$^{-/-}$) flies (3 weeks old) to attractive (putrescine, 2,3-butanedione) and aversive
944 odors (benzaldehyde, 3-octanol) in the T-maze assay suggests that autophagy is not involved in
945 innate olfaction. Box plot shows median and upper/lower quartiles (n = 8, 60 flies/trial 30 ♀ and
946 30 ♂). (B) Box plots show olfactory preference index (P.I.) of 1 week old transgenic flies
947 carrying an *in vivo* RNAi construct to knock-down SOD2 pan-neuronally under the control of
948 *elav-Gal4 (elav-Gal4;UAS-SOD2-RNAi)* and their genetic controls to 2,3-butanedione,
949 benzaldehyde and 3-octanol in the T-maze assay. P-values were calculated via one-way
950 ANOVA with the Bonferroni multiple comparison posthoc test (A) or with the t-test (B) (ns >
951 0.05, *p ≤ 0.05, **p ≤ 0.01, ***p ≤ 0.001).
952
953 **Figure 4 - Figure Supplement 2.** (A) RNA-seq expression of the total number of genes
954 expressed in the 1 week (orange) and 7 weeks (grey) fly antenna. Y-axis represents total
955 number of genes expressed in the antenna, while the x-axis shows the age of flies in weeks.

956 Doughnut chart represents the number of genes upregulated (green) and downregulated (light
957 brown) in 7 weeks old antennae compared to one week old. (B) RNA-seq expression of the total
958 number of genes expressed in 1 week (orange) and 7 weeks (grey) old fly brains. Y-axis
959 represents total number of genes expressed in the brain, while the x-axis shows the age of flies
960 in weeks. Doughnut chart represents the number of genes upregulated (green) and
961 downregulated (light brown) in 7 weeks old brains, compared to one week old. (C) Volcano plot
962 of RNA-sequencing data of selected genes displaying the genes that are downregulated and
963 upregulated in 7 weeks old antennae and brains, respectively. Only genes above the cutoff of –
964 log10 (p-value adjusted (padj)) are considered significantly changed. Note that SOD1 and 2
965 expression does not change significantly in the antenna. Both genes, however, are significantly
966 downregulated in the brain of old flies. (D) Box plot show olfactory preference index (P.I.) of 1
967 week old transgenic flies expressing a knockdown-construct of SOD2 pan-neuronally under the
968 mature neuron driver *nsyb (nsyb-Gal4;UAS-SOD2-RNAi)* and their genetic controls to 2,3-
969 butanedione, benzaldehyde and 3-octanol in the T-maze assay. Box plot shows median and
970 upper/lower quartiles (n = 8, 60 flies/trial 30 ♀ and 30 ♂). All p-values were calculated via two-
971 way ANOVA with the Bonferroni multiple comparison posthoc test (ns > 0.05, *p ≤ 0.05, **p ≤
972 0.01, ***p ≤ 0.001).
973
974 **Supplementary File 1**. Genes upregulated in brains of 7 weeks old flies vs. brains of 1 week
975 old flies organized by GO (gene ontology) terms.
976
977 **Supplementary File 2**. Genes downregulated in brains of 7 weeks old flies vs. brains of 1 week
978 old flies organized by GO (gene ontology) terms.
979
980 **Figure 4 - Figure Supplement 3.** (A) Survivorship of flies with RNAi knockdown of SOD2 in
981 projection neurons using the *GH146-Gal4 (GH146-Gal4;UAS-SOD2-RNAi)* and their genetic

982 control (*Gh146-Gal4*) shown in line graphs. Y-axis represents % survivorship, while the x-axis
983 shows the age of flies in weeks (n=200 ± SEM). (B) Survivorship of flies with overexpression of
984 SOD2 in PNs using the GH146-Gal4 *(GH146-Gal4;UAS-SOD2)* and their genetic controls
985 (*GH146-Gal4*) shown in the line graph. Y-axis represents % survivorship, while the x-axis shows
986 the age of the flies in weeks (n=100 ± SEM, 3 replicates). (C) Survivorship of flies raised from
987 day 1 on Resveratrol (grey line), *L. plantarum* (lime green), and standard fly food (magenta). Y-
988 axis represents % survivorship, while the x-axis shows the age of flies in weeks (n=100 ± SEM,
989 3 replicates). Please note that these survival curves are not intended to test the effect of the
990 treatment on lifespan, but rather to correlate the lifespan of individual test and control groups
991 with their behavioral performance to exclude unspecific effects of general health.
992
993 **Figure 6 - Figure Supplement 1.** (A) Box plots show P.I.s of 1 week old (orange bars) and 7
994 weeks old (grey bars) transgenic flies overexpressing SOD2 exclusively in projection neurons
995 (PNs) *(GH146-Gal4;UAS-SOD2)* and their genetic controls in response to attractive (putrescine)
996 and aversive (benzaldehyde) odors. (B) Box plots show P.I.s of 1 week old (orange bars) and 7
997 weeks old (grey bars) transgenic flies overexpressing SOD2 under the control of *ORCO-Gal4* in
998 OSNs *(ORCO-Gal4;UAS-SOD)* and their genetic controls in response to attractive (putrescine)
999 and aversive (3-octanol) odors. (C) Box plots show preference of 1 week old and 7 weeks old
1000 flies raised on standard fly food (first 2 bars) and 7 weeks old flies raised on standard fly food
1001 mixed with Resveratrol (third grey bar) in response to attractive (putrescine) and aversive
1002 (benzaldehyde) odors. All p-values were calculated via t-test (ns > 0.05, *p ≤ 0.05, **p ≤ 0.01,
1003 ***p ≤ 0.001). In all figures, asterisks above a single bar refer to p-values of comparison to the
1004 control (7 weeks old flies in 2nd bar). (D) Box plots show 1-2 weeks old flies raised on standard
1005 food with solvent or on standard fly food supplemented with Resveratrol for 1 week. There is no
1006 significant difference between the treated and control flies (n=8). (E) Box plots show untreated
1007 and treated (flies were inoculated with the indicated bacterial strain after being pretreated to

1008 become germfree) 1 week old (light (treated) and dark orange (not germfree, standard
1009 conditions as in all other experiments before) and 7 weeks old (dark and light grey) flies.
1010 Treated flies were inoculated with *Lactobacillus plantarum NI202877, L. plantarum WJL,*
1011 *Acetobacter pomorum (A.p.),* while control flies were just raised on standard fly food. P.I.s of
1012 flies to attractive (putrescine) and aversive (benzaldehyde, 3-octanol) odors is shown. All p-
1013 values were calculated via two-way ANOVA with the Bonferroni multiple comparison posthoc
1014 test (ns > 0.05, *p ≤ 0.05, **p ≤ 0.01, ***p ≤ 0.001). Asterisks above a single bar refer to p-
1015 values of comparison to the control (7 weeks old treated control). Box plot show median and
1016 upper/lower quartiles (n = 8, 60 flies/trial 30 ♀ and 30 ♂).
1017

Figure 1

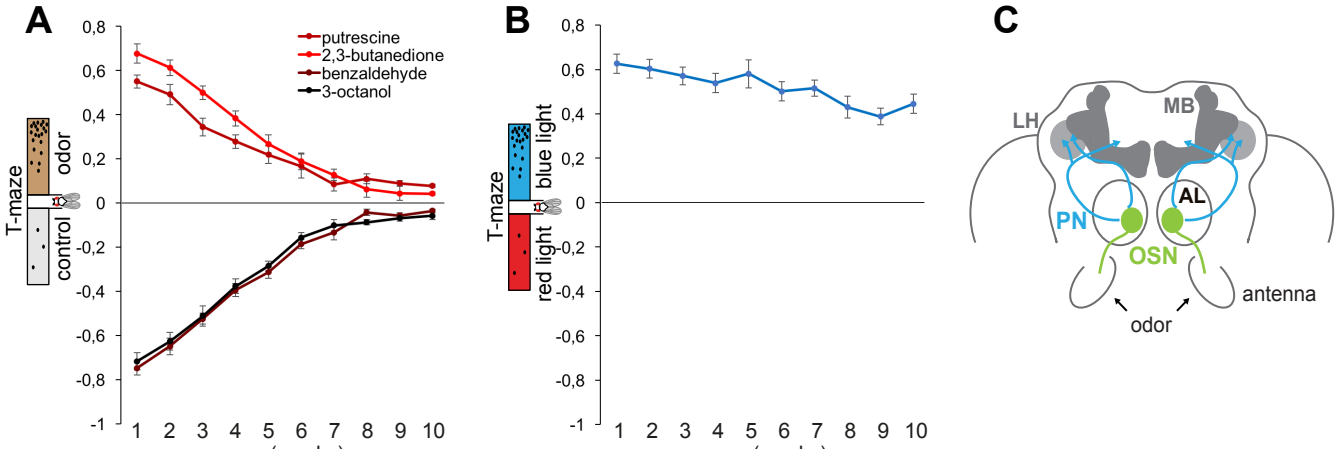
A
putrescine
2,3-butanedione
benzaldehyde
3-octanol
T-maze
odor
control
0,8
0,6
0,4
0,2
0
-0,2
-0,4
-0,6
-0,8
-1
1 2 3 4 5 6 7 8 9 10
age (weeks)
B
T-maze
blue light
red light
0,8
0,6
0,4
0,2
0
-0,2
-0,4
-0,6
-0,8
-1
1 2 3 4 5 6 7 8 9 10
age (weeks)
C
LH
MB
AL
PN
OSN
antenna
odor

Figure 2

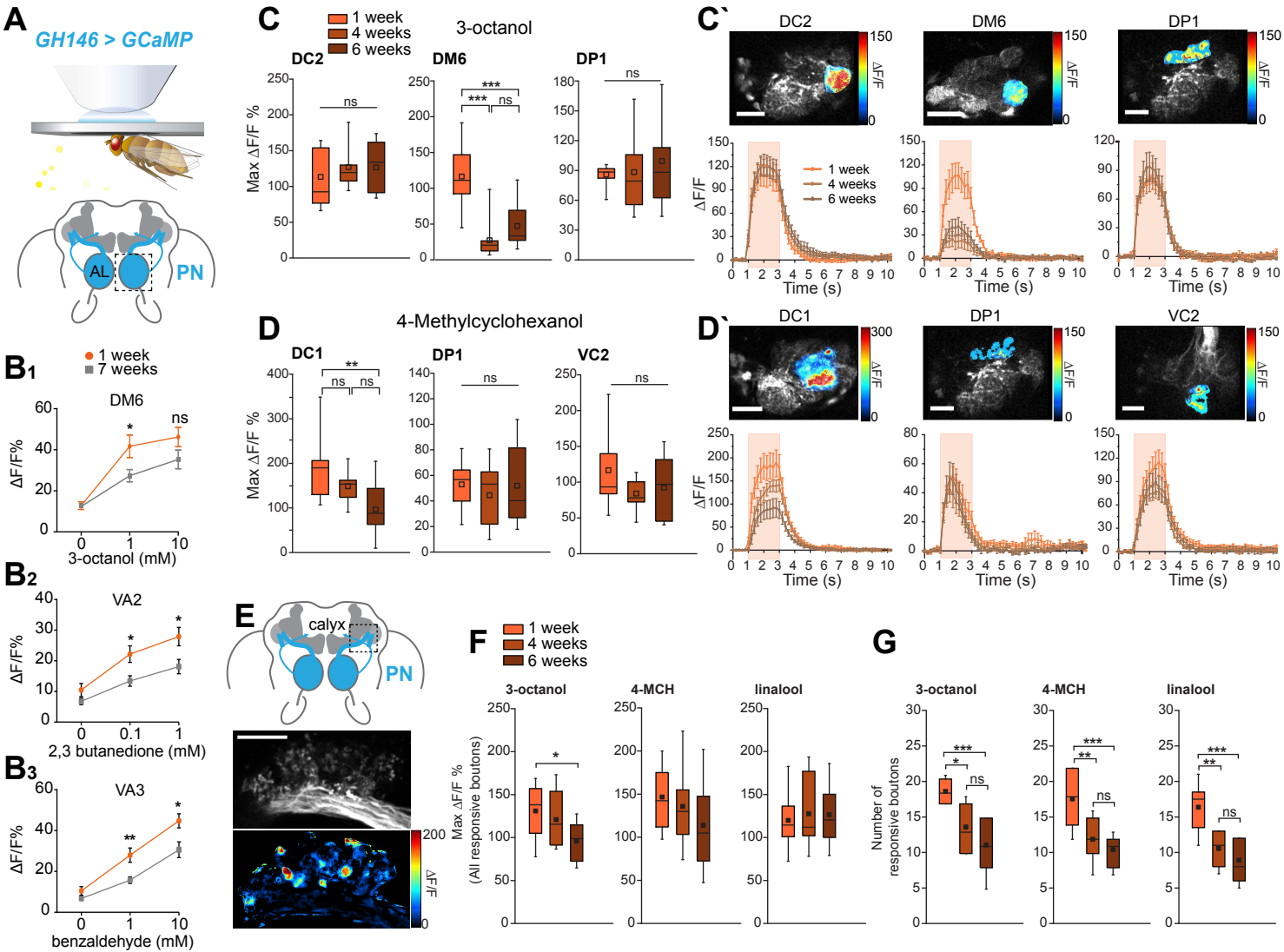
A
GH146 > GCaMP
AL
PN
B1
1 week
7 weeks
DM6
ΔF/F%
3-octanol (mM)
B2
VA2
2,3 butanedione (mM)
B3
VA3
benzaldehyde (mM)
C
1 week
4 weeks
6 weeks
3-octanol
DC2
DM6
DP1
Max ΔF/F %
C`
Time (s)
D
4-Methylcyclohexanol
DC1
DP1
VC2
D`
E
calyx
PN
F
3-octanol
4-MCH
linalool
Max ΔF/F %
(All responsive boutons)
G
Number of responsive boutons

Figure 3

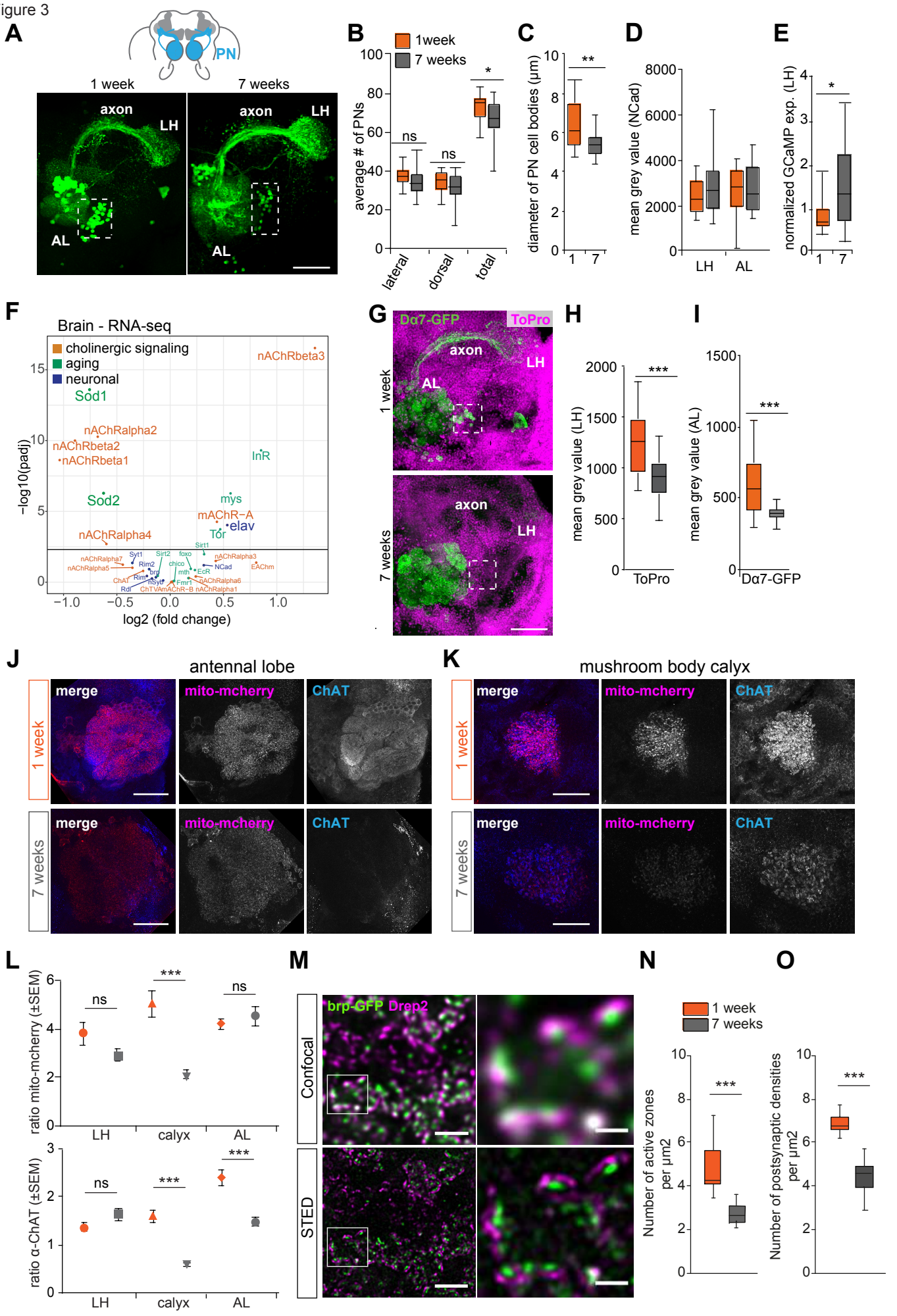
A
PN
1 week
7 weeks
axon
LH
AL
B
1week
7 weeks
average # of PNs
ns
ns
*
lateral
dorsal
total
C
diameter of PN cell bodies (µm)
**
1
7
D
mean grey value (NCad)
LH
AL
E
normalized GCaMP exp. (LH)
*
1
7
F
Brain - RNA-seq
cholinergic signaling
aging
neuronal
nAChRbeta3
Sod1
nAChRalpha2
nAChRbeta2
nAChRbeta1
InR
Sod2
mys
mAChR-A
elav
Tor
nAChRalpha4
−log10(padj)
log2 (fold change)
G
Dα7-GFP
ToPro
axon
LH
AL
1 week
7 weeks
H
mean grey value (LH)
***
ToPro
I
mean grey value (AL)
***
Dα7-GFP
J
antennal lobe
1 week
7 weeks
merge
mito-mcherry
ChAT
K
mushroom body calyx
1 week
7 weeks
merge
mito-mcherry
ChAT
L
ratio mito-mcherry (±SEM)
ns
***
ns
LH
calyx
AL
ratio α-ChAT (±SEM)
ns
***
***
LH
calyx
AL
M
Confocal
STED
brp-GFP Drep2
N
1 week
7 weeks
Number of active zones per µm2
***
O
Number of postsynaptic densities per µm2
***

Figure 4

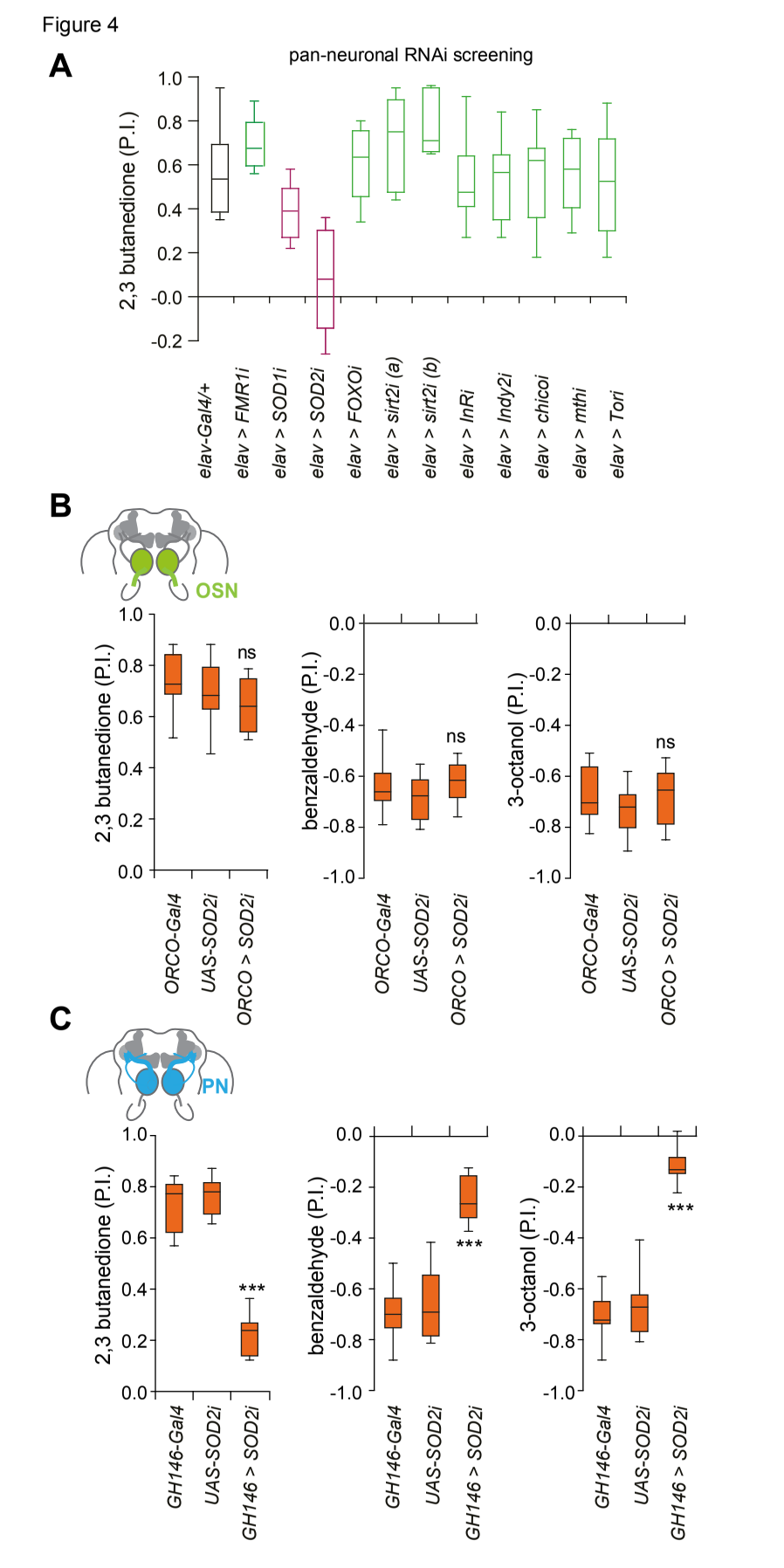
A
pan-neuronal RNAi screening
2,3 butanedione (P.I.)
1.0
0.8
0.6
0.4
0.2
-0.0
-0.2
elav-Gal4/+
elav > FMR1i
elav > SOD1i
elav > SOD2i
elav > FOXOi
elav > sirt2i (a)
elav > sirt2i (b)
elav > InRi
elav > Indy2i
elav > chicoi
elav > mthi
elav > Tori
B
OSN
2,3 butanedione (P.I.)
benzaldehyde (P.I.)
3-octanol (P.I.)
ns
ORCO-Gal4
UAS-SOD2i
ORCO > SOD2i
C
PN
***
GH146-Gal4
UAS-SOD2i
GH146 > SOD2i

Figure 5

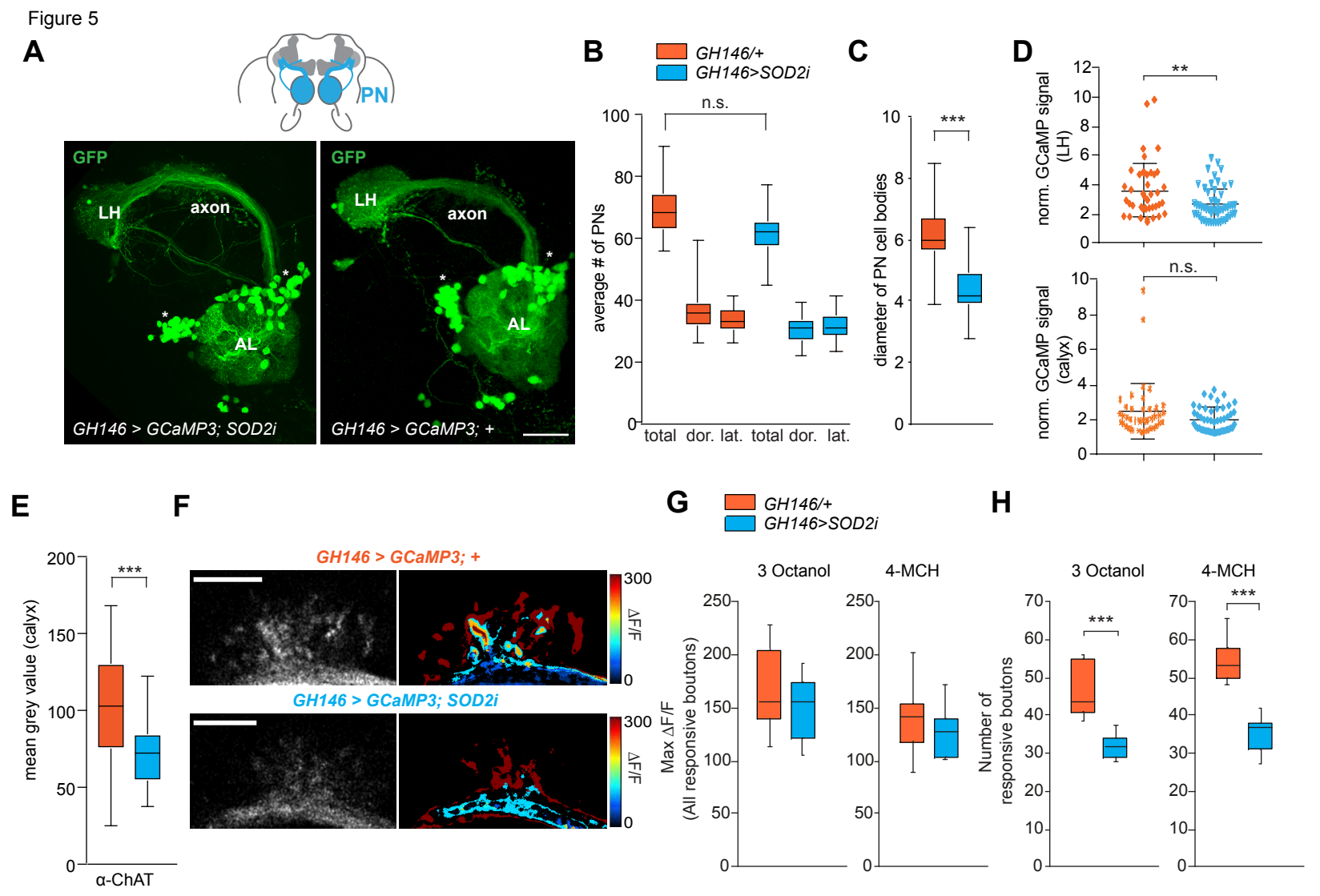
A
PN
GFP
LH
axon
AL
GH146 > GCaMP3; SOD2i
GH146 > GCaMP3; +
B
GH146/+
GH146>SOD2i
n.s.
average # of PNs
total dor. lat. total dor. lat.
C
***
diameter of PN cell bodies
D
**
norm. GCaMP signal (LH)
n.s.
norm. GCaMP signal (calyx)
E
***
mean grey value (calyx)
α-ChAT
F
GH146 > GCaMP3; +
GH146 > GCaMP3; SOD2i
ΔF/F
G
GH146/+
GH146>SOD2i
3 Octanol
4-MCH
Max ΔF/F (All responsive boutons)
H
3 Octanol
4-MCH
***
Number of responsive boutons

Figure 6

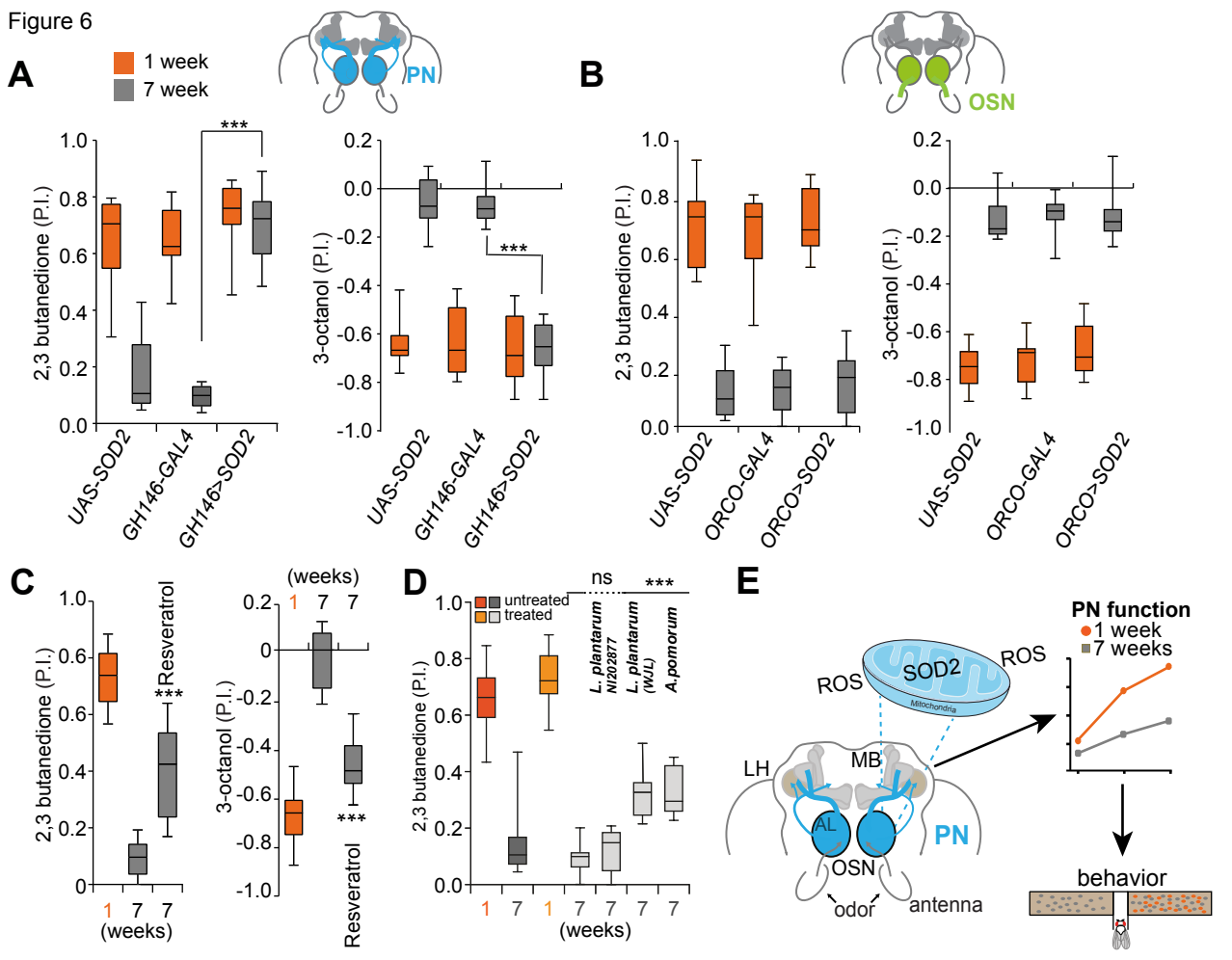
A
1 week
7 week
PN
***
2,3 butanedione (P.I.)
3-octanol (P.I.)
UAS-SOD2
GH146-GAL4
GH146>SOD2
B
OSN
ORCO-GAL4
ORCO>SOD2
C
Resveratrol
(weeks)
D
untreated
treated
ns
L. plantarum NI202877
L. plantarum (WJL)
A.pomorum
E
PN function
1 week
7 weeks
ROS
SOD2
Mitochondria
LH
MB
AL
OSN
odor
antenna
behavior

Fig. 1- Fig. Supplement 1

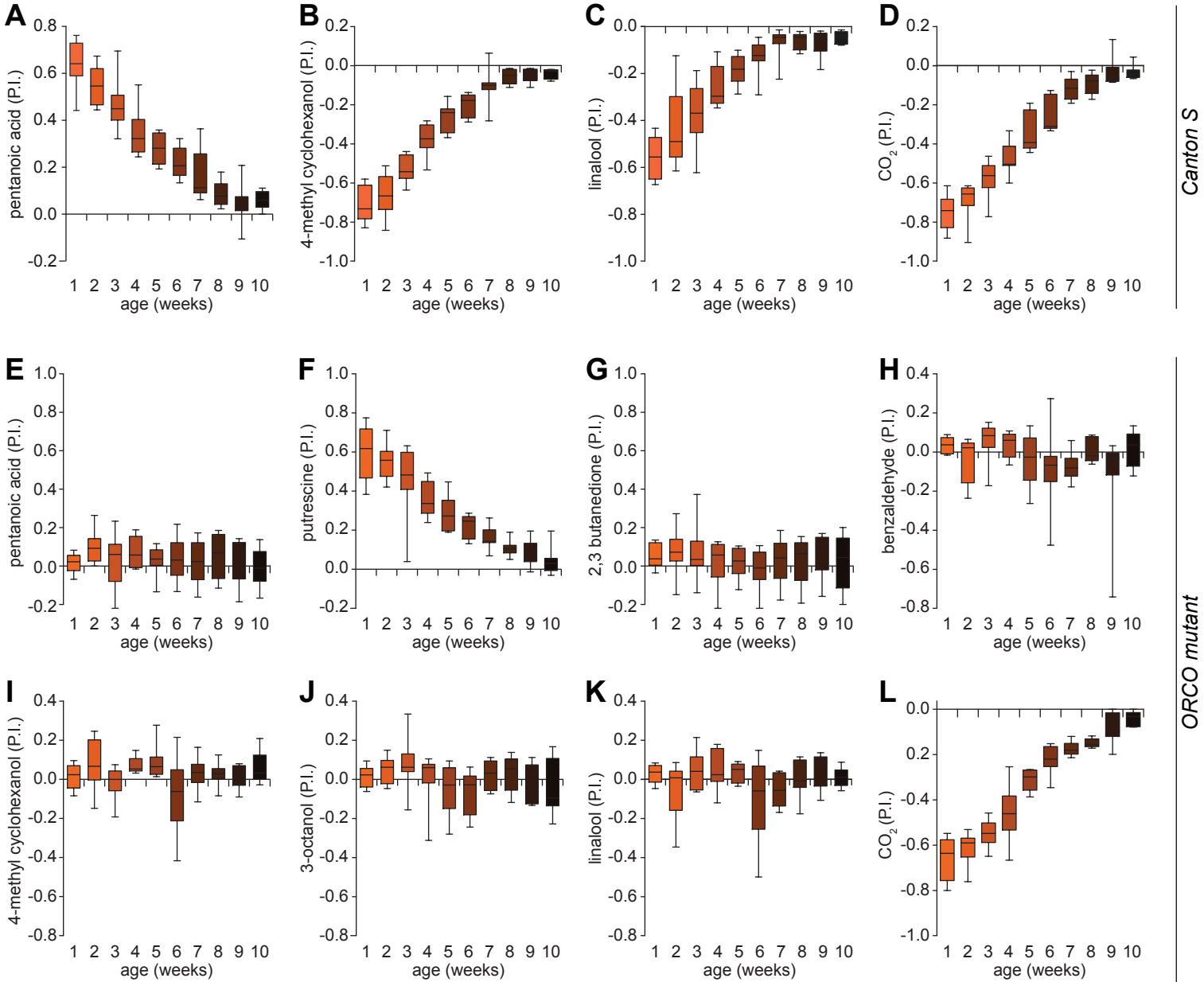

Fig. 2- Fig. Supplement 1

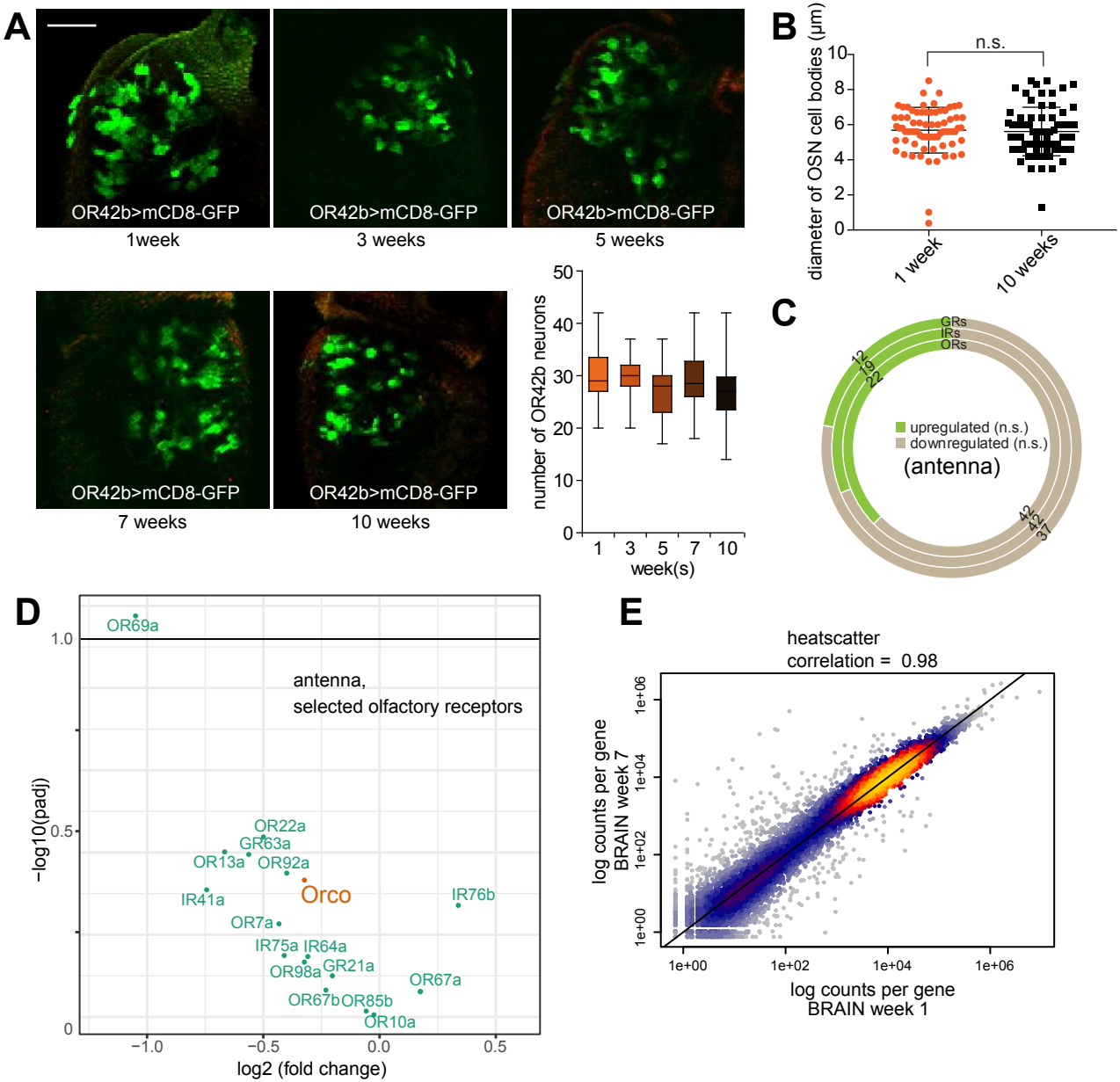

Fig. 2- Fig. Supplement 2

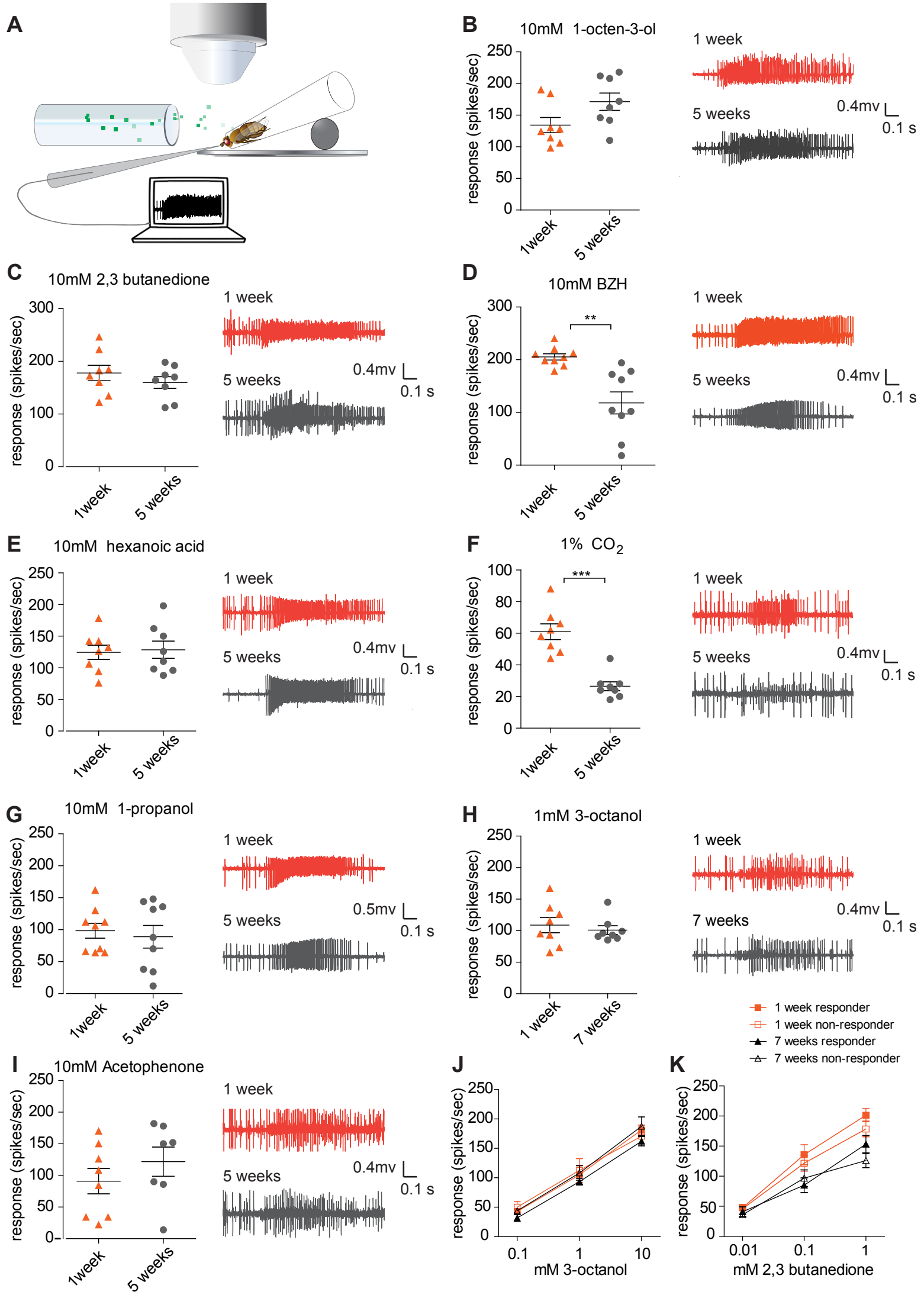

Fig. 2- Fig. Supplement 3

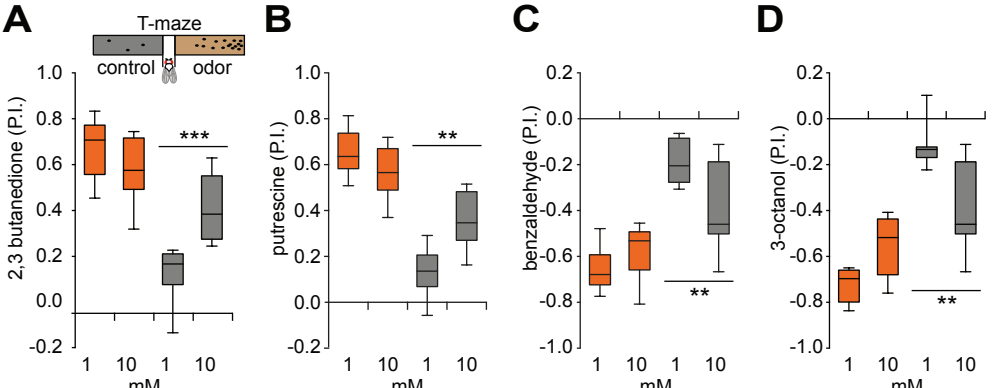

Fig. 4- Fig. Supplement 1

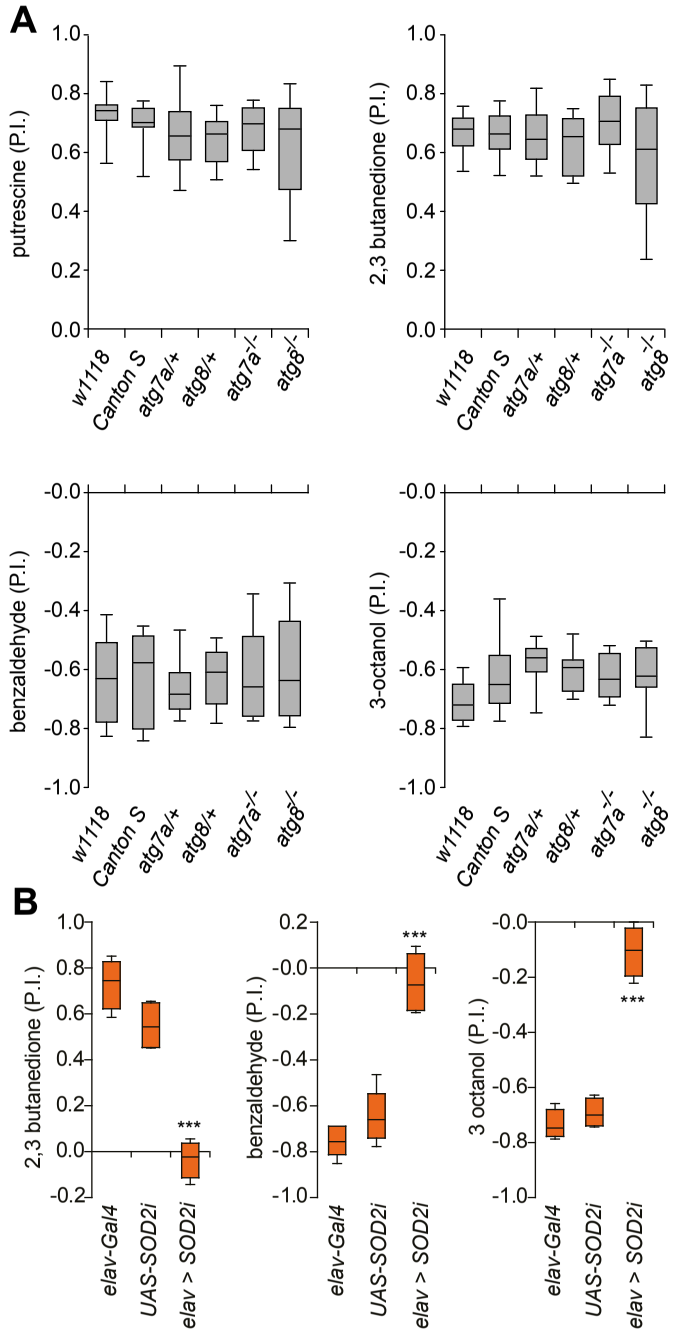

Fig. 4- Fig. Supplement 2

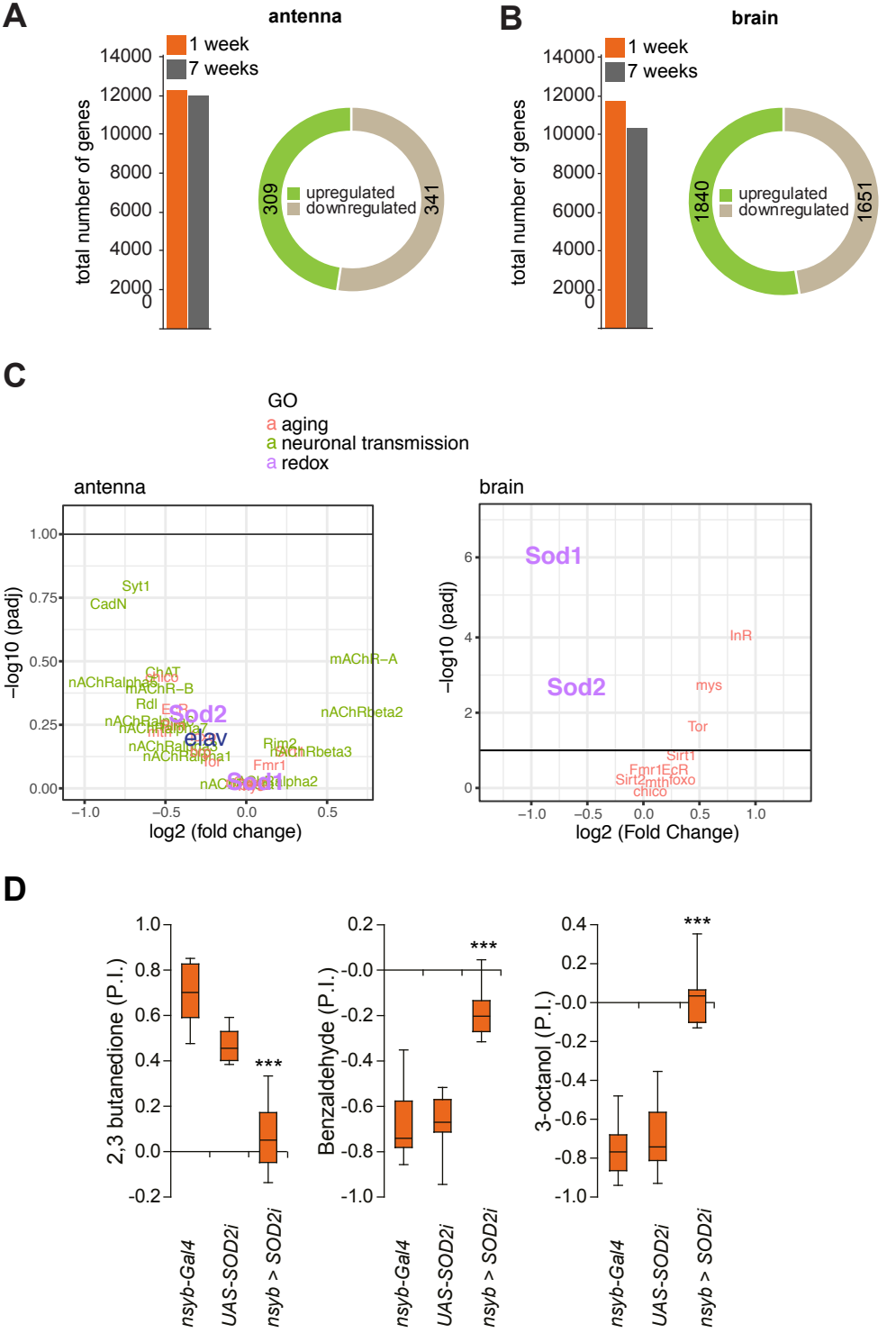

Fig. 4- Fig. Supplement 3

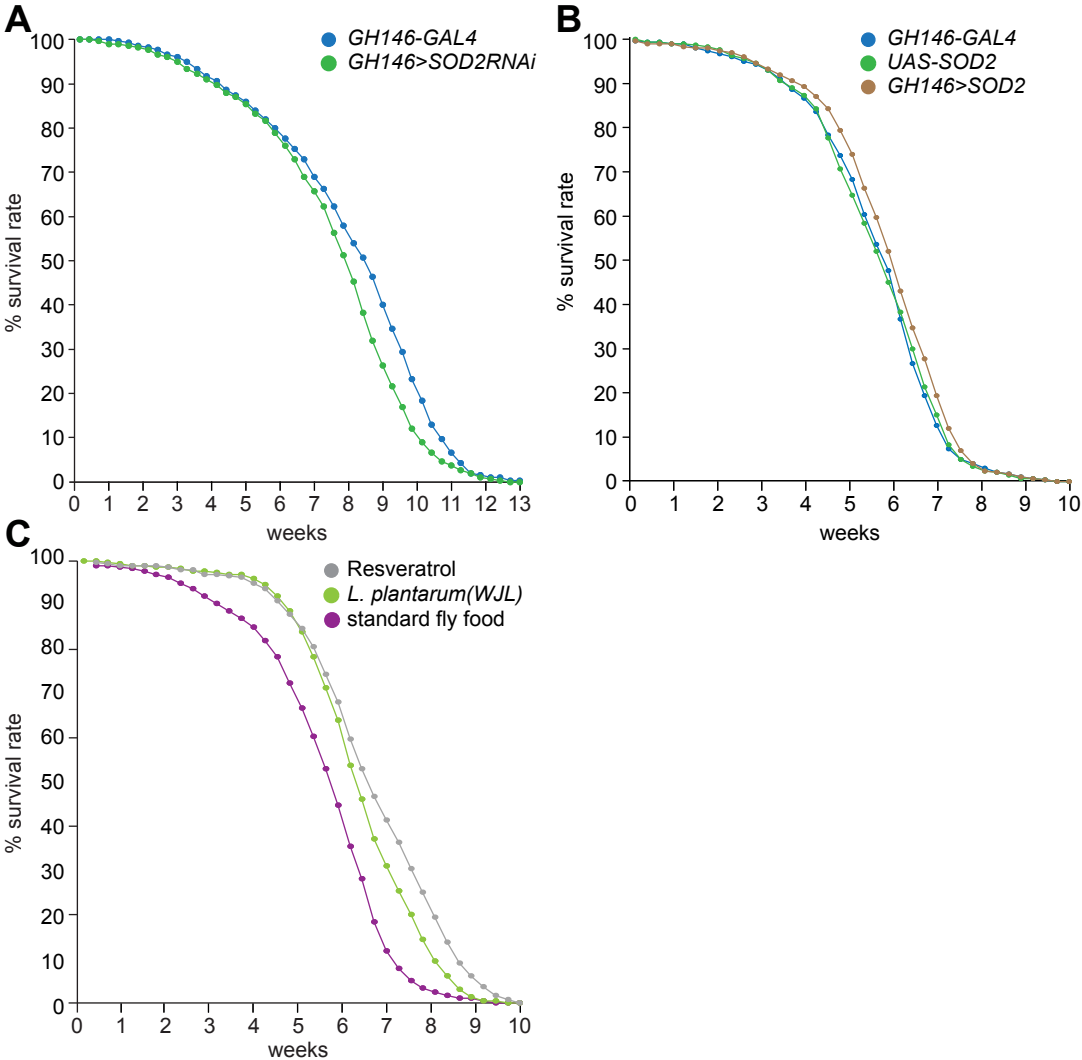

Fig. 6 - Fig. Supplement 1